Cement and Concrete Research 130 (2020) 105976

Contents lists available at ScienceDirect

Cement and Concrete Research

journal homepage: www.elsevier.com/locate/cemconres

The effect of artificial leaching with HCl on chloride binding in ordinary Portland cement paste

Petter Hemstad*, Alisa Machner, Klaartje De Weerdt

Department of Structural Engineering, NTNU, Richard Birkelands vei 1a, 7491 Trondheim, Norway

ABSTRACT

This study investigates how the pH in the pore solution influences the chloride binding in Portland cement pastes. Cement paste samples were exposed to NaCl, $CaCl_2$ and HCl solutions. The mechanisms of changes in chloride binding were investigated using a wide variety of techniques both for the liquid and solid phase. Lowering the pH from 13 to 12 with $CaCl_2$ or HCl greatly increased chloride binding compared to NaCl, which was associated with increased amounts of chlorides in the AFm-phases. Lowering the pH below 12 lead to reduced chloride binding in part due to dissolution of AFm. Chloride binding approached zero at a pH of 9. The influence of C-S-H on changes in chloride binding could not be conclusively determined. The impact of leaching and low pH on chloride binding is key to explaining the peaking behaviour of chloride profiles in concrete submerged in chloride containing solutions like sea water.

1. Introduction

Chloride induced reinforcement corrosion is one of the major deterioration mechanisms for reinforced concrete structures exposed to chlorides. Chlorides will over time be transported into the concrete, and at a certain point a critical concentration of chlorides at the steel reinforcement will be reached. At this point the reinforcement is susceptible to suffer from pitting corrosion [1]. Corrosion can reduce the cross section of the reinforcement and cause cracking and spalling of the concrete cover, severely impacting the structural performance of the reinforced concrete [2]. Service life models commonly define the time when corrosion initiates as the end of service life for structures exposed to external chlorides [3].

Models for service life prediction are often used to calculate the relationship between the thickness of the concrete cover and the time till corrosion initiation [3–6]. Accurate models allow for better selection of thickness, composition and cement content for the concrete cover. This can be very helpful for designing and constructing durable concrete structures, minimizing the environmental impact of the structure by lowering the amount of repair and maintenance.

Service life models commonly use experimental chloride profiles to determine a Fickian diffusion coefficient for the chlorides in the concrete. This is achieved by fitting experimentally obtained chloride profiles in concrete to a solution of Fick's law [3,7]. However, the chloride profiles appear non-Fickian due to the complex interactions between the chloride ions and the concrete. The profiles show a peaking behaviour, where the chloride content is higher just below the surface of the concrete than at the surface itself. This peaking behaviour becomes more prominent as the exposure time increases [8,9]. For concrete in the tidal zone the peaking has been attributed to convection transport caused by wetting/drying cycles [8], however the peaking behaviour is also observed in submerged concrete and mortar where diffusion is the main transport mechanism [9–12]. Fig. 1 shows an example of the development of this peak over time in submerged Portland cement mortars [9]. The cause of the peaking in submerged concrete is currently unknown. Service life models generally ignore the outer sections of the chloride profile to improve the fitting of the diffusion model [5]. However, by taking into account the phase changes caused by sea water exposure, new models might be able to explain the peaking behaviour and incorporate the outer sections, thereby enabling more accurate predictions of chloride ingress.

Chlorides and several other ions will penetrate the concrete during exposure to sea water. These ions cause a series of phase changes with varying penetration depths [12–14]. Additionally, the near neutral pH of the sea water will eventually lower the pH of the pore solution. In this study the combination of phase changes and lowered pH caused by sea water exposure is referred to as leaching.

The results of a previous study indicated that the lowered pH caused by leaching might be the main cause for the peaking behaviour of the chloride profiles [15,16]. Exposing cement pastes to NaCl and afterwards lowering the pH by adding HCl lead to increased chloride binding whilst the pH was above 12. When the pH dropped to 11, the chloride binding of the paste almost completely vanished. The conclusion was that the peak in the chloride profiles occurs due to harsh leaching, drastically lowering the chloride binding of the outmost sections and thereby reducing the total chloride content. Mild leaching

* Corresponding author.
E-mail address: petter.hemstad@ntnu.no (P. Hemstad).

https://doi.org/10.1016/j.cemconres.2020.105976
Received 30 September 2019; Received in revised form 9 January 2020; Accepted 10 January 2020

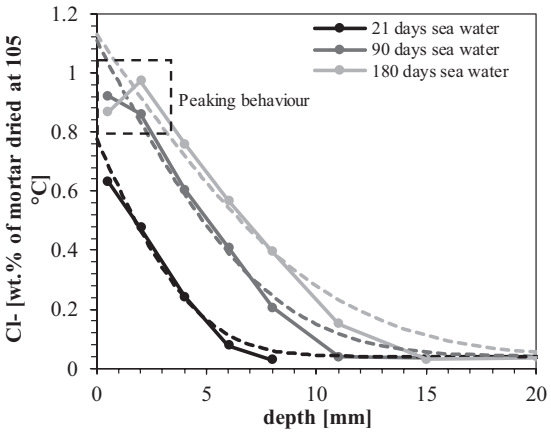

Fig. 1. Experimentally obtained chloride profiles from Portland cement mortars after submersion for 21, 90, and 180 days in sea water (solid lines), and models found by fitting solutions to the error function of Fick's law to the experimental profiles (dashed lines).
Adapted from [9].

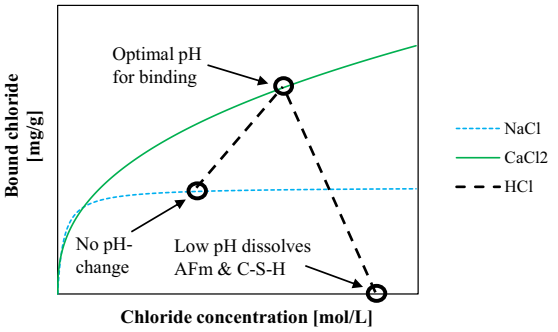

Fig. 2. Schematic drawing of the expected progression of the chloride binding for exposure of cement paste to NaCl, $CaCl_2$ and NaCl + HCl, as a function of the chloride concentration in the exposure solution [16].

slightly deeper in the concrete leads to increased chloride binding, resulting in the peaking of the chloride profile. However, the study was unable to experimentally verify the mechanisms that lead to changes in chloride binding. This was partially due to the cement paste having been cured at 60 °C before storage at 20 °C. The phase assemblage was affected as a result [17,18], preventing the detection of Friedel's salt ($3CaO{\cdot}Al_2O_3{\cdot}CaCl_2{\cdot}10H_2O$). In addition, the solvent exchange used to remove free water resulted in crystallization of NaCl, which meant the investigated solids were not fully representative. Another assumption made during the previous study was that the volume of free water provided by the cement paste remained constant upon acid exposure. Considering that hydrate phases such as portlandite ($Ca(OH)_2$, CH in shorthand notation) are dissolving and releasing water, this assumption is incorrect.

It could be expected that the pH of the pore solution would affect the chemical and physical binding of chlorides in cement. The main chloride binding phase, Friedel's salt, is more stable at a pH slightly lower than the 13–13.5 which is common in pore solutions, suggesting increased chemical chloride binding for small drops in pore solution pH [19]. Friedel's salt is however unstable when the pH approaches neutral [20]. The solid solutions between Friedel's salt and hydroxyl AFm [21] is also likely to have an increase in the Cl/OH-ratio as the pH (and thus the concentration of OH^- in the pore solution) decreases. This would contribute to increased chloride binding even if the amount of AFm remains constant.

For the physical binding, Cl^- and OH^- ions can accumulate in the diffuse layer of the C-S-H. Although not directly adsorbed on the surface, they will behave similarly to competitively adsorbing ions [22,23]. According to Tritthart [24], the physical binding of Cl^- will be increased if the concentration of the competing hydroxyl ions is reduced, i.e. as the pH is decreased. However, this has been studied for chlorides introduced in the mixing water, which changes the microstructure of the cement paste [25,26]. It has been observed exposing cement paste to $CaCl_2$ decreases the pH of the pore solution and increases chloride binding in addition to increasing the calcium concentration [24,27–30]. Together with the effect of pH on the accumulation of chloride ions, the increased calcium concentration is likely to influence the chloride binding. Calcium can adsorb on the surface of the C-S-H, reversing its surface charge. More adsorbed calcium increases the positive charge and thereby the accumulation of chloride ions in the diffuse layer [22,27]. As pointed out by previous studies, there is an inevitable link between the pH and calcium concentration of the pore solution [27,29]. It is therefore difficult to determine the individual contribution of each factor to changes in the chloride binding of cement pastes.

The physical binding of chlorides might also be related to the zeta potential of the cement paste. Pointeau et al. [31] studied the effect of degradation via leaching on the zeta potential of hydrated cement pastes. They found that the zeta potential of a CEM-I paste increased from negative values (ca. -20 mV) to positive values (ca. 20 mV) for a pH dropping from 13.3 to 12.6. At pH 12.6 it peaks, before decreasing to negative values with point of zero charge near pH 11.7. The results from Pointeau et al. point to a possible effect that lowering pH can have on the physical chloride binding of cement pastes. Small drops in pH such as those caused by $CaCl_2$ exposure lead a positive zeta potential for the C-S-H, resulting in increased physical chloride binding. Large drops in pH caused by severe leaching might lead to a decrease in zeta potential, fully reversing the sign of the surface charge and thereby disabling the physical binding of chlorides by the C-S-H.

Following the work by Tritthart [24], our previous study [16] investigated the influence of pH on chloride binding by adding HCl to a well-hydrated Portland cement paste. Fig. 2 shows the working hypothesis of the previous and the present studies regarding the chloride binding during HCl exposure. The chloride binding isotherms of NaCl and $CaCl_2$ are already well documented [24,27–30], and generally follow similar trends as those illustrated in Fig. 2. Exposure to increasing concentrations of $CaCl_2$ generally increases the chloride binding of a cement paste, much more so than for similar concentrations of NaCl. Above a certain chloride concentration, the chloride binding isotherm for NaCl reaches a plateau and ceases to increase. If there was no influence of pH on chloride binding, the isotherms for NaCl and HCl should be the same. To make sure any difference in chloride binding between the HCl and NaCl isotherms are due to lower pH and not increased chloride concentration, the starting point for HCl additions in [16] was selected to be on this plateau. Our hypothesis is that the chloride binding during HCl-exposure will initially increases for small additions of HCl. It would continue to increase until the point where Friedel's salt would start to dissolve and the physical binding by C-S-H would start to decrease. Further additions of acid and reductions in pH would eventually lead to total dissolution of chloride binding phases.

Adding HCl to the cement paste brings some unique challenges compared to NaCl and $CaCl_2$, as direct addition of acid to the cement paste would lead to rapid and inhomogeneous dissolution. Instead of adding all the exposure solution at once, the acid can be added in smaller doses over time which would also prevent sharp drops in pH and local inhomogeneities [16]. Using HCl does however enable lowering the pH of the pore solution without introducing new species to the system. Adding HNO_3 could for instance lead to complications by forming NO_3^--AFm at the expense of Friedel's salt [32].

This study expands on the work in Machner et al. [16]. The mechanisms and magnitude of chloride binding in Portland cement paste

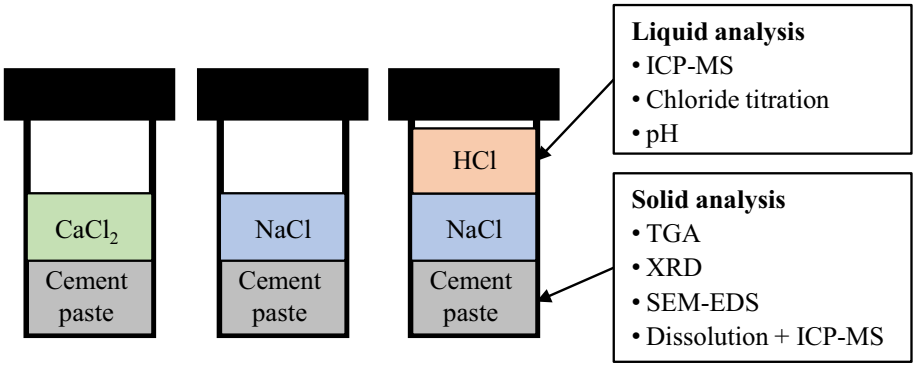

Fig. 3. Illustration of sample setup and overview of the performed analyses. Three sets of similar samples were prepared, all of which started by adding well-hydrated cement paste to a centrifuge tube. Two of the sets were exposed to the same volume of $CaCl_2$ or NaCl with varying chloride concentration. The third set was exposed to 1.5 mol/L NaCl before 4 mol/L HCl was added gradually to lower pH. All samples were analysed for chloride concentration using $AgNO_3$-titration, ICP-MS and a pH-probe. The solids of select samples were also analysed using TGA, XRD, SEM-EDS and dissolution coupled with ICP-MS.

at low pH were thoroughly investigated, accounting for the dissolution of paste and the changes in solution volume. Well-hydrated ordinary Portland cement pastes were exposed to a NaCl solution, before the pH in the solution was lowered by adding HCl. 24 samples were acidified to reach 9 different levels of pH, and the chloride binding of the pastes at each level was determined. The concentrations of different elements in the exposure solution was studied using inductively coupled plasma mass spectrometry (ICP-MS) The phase assemblage of the cement pastes was then investigated using thermogravimetric analysis (TGA), X-ray diffraction (XRD), scanning electron microscopy with energy dispersive spectroscopy (SEM-EDS) and ICP-MS to elucidate the mechanisms behind the changes in chloride binding.

2. Methods and materials

In this section the sample preparation and experimental procedures are detailed. Fig. 3 illustrates the sample setup and gives an overview of the analyses which were performed. More detailed description of the samples follows in Sections 2.1 and 2.2, whilst the analyses are detailed in Sections 2.3 and 2.4. Finally, Section 2.6 describes the thermodynamic model used to model phase assemblage and pore solution in the samples.

2.1. Materials and sample preparation

Table 1 gives the chemical composition of the Portland cement (supplied by Norcem AS) used in this study, as determined by X-ray fluorescence.

A total of 2.16 kg cement paste was prepared with the same methodology as in [16]. This method yields a cement paste with high surface area and degree of hydration. The pore solution will therefore readily equilibrate with exposure solutions, and there should be little effect of additional hydration after exposure. Four paste mixes with 360 g cement and 180 g deionized water (w/c = 0.5) per mix were blended in a Braun MR5550CA high shear mixer. Each batch was blended at high speed for 30 s, then after 5 min of rest they were blended again for 60 s. The mixes were divided evenly into 125 mL plastic bottles, and each bottle was sealed with screw-on lids and parafilm. The sealed bottles were then stored at 20 °C for 3 months inside plastic boxes, which were filled with water up the bottle necks of the 125 mL bottles. After this period of initial curing, the pastes were cut out of the bottles and crushed in a jaw crusher to reach particle sizes below 1 mm. Any particles larger than 1 mm were crushed in a rotating disc mill until they also were below 1 mm in diameter. The ground cement pastes were distributed into 1 L polypropylene bottles, to which 30% of the cement paste mass (mass%) of deionized water was added. These 1 L bottles were sealed with lids and parafilm and stored at 20 °C. One week after sealing the pastes were all combined, homogenized and distributed into 125 mL polypropylene bottles. The pastes were then stored for 4 months before chloride exposure. With the original w/c-ratio of 0.5 and the additional 30 mass% water, the final paste had a measured total w/c-ratio of 0.78.

To clarify the terminology, the cement paste will be referred to using the terms described in Eq. (1).

$$m_{sample} = m_{paste} + m_{H_2O} = (m_{cement} + w) + m_{H_2O} \quad (1)$$

Here m_{sample} is the mass of well-hydrated cement paste in each sample. This paste can be split up into two parts: m_{paste} is the mass of cement paste with no free water, and m_{H2O} is the mass of free water originating from the well-hydrated paste. The mass of cement paste can again be split into two parts, the first being the mass of cement (m_{cement}) and the other being the mass of bound water (w). Some values were measured as volume or mass percentages, which will be indicated with a percentage sign as a subscript (i.e. $w_{\%}$ for mass% of bound water).

2.2. Exposing paste to NaCl, $CaCl_2$ and HCl

All the exposed samples were prepared by weighing in 15 ± 0.01 g of the well-hydrated cement paste in 50 mL centrifuge tubes. The samples were divided into three different types of chloride exposure: NaCl-isotherm, $CaCl_2$-isotherm and HCl acidification (see Fig. 3). For both the isotherm-groups, 20 mL of a NaCl or $CaCl_2$ solution with various concentrations was added to the sample tubes. These chloride solutions were made using deionized water and NaCl or $CaCl_2{\cdot}2H_2O$ (laboratory grade salts, supplied by Merck) to reach Cl^--concentrations of 0.25, 0.5, 1, 1.5, 2 and 3 mol/L. These samples were then stored for four weeks to equilibrate.

After the equilibration period, the acidification procedure for the HCl-samples using 4 mol/L HCl was initiated. Three samples were used to determine how the pH of the pore solution changed as increasing volumes of acid were added. These are referred to as “progression samples” as they show how progressive exposure to acid changes the pH of the exposure solution. The acid was added to the samples once per working day in steps of increasing volume. First, 10 steps of 0.25 mL, then 5 steps of 0.5 mL, followed by 7 steps of 1 mL and finally 4 steps of 2 mL, for a total of 20 mL. Before each addition, the samples were centrifuged, creating a larger volume of solution shielding the paste from direct acid exposure. The pH of the exposure solution was

Table 1
Chemical composition of the Portland cement (PC) used here, as determined with XRF [% of total ignited mass]. The same cement was used in [16].

	SiO_2	Al_2O_3	TiO_2	MnO	Fe_2O_3	CaO	MgO	K_2O	Na_2O	SO_3	P_2O_5
PC	19.91	5.15	0.28	0.06	3.42	62.73	2.34	1.09	0.48	3.16	0.11

measured 5–10 min and one working day after each acid addition (respectively "instant pH" and "pH at EQ" in Fig. 5). The aim of these samples was only to get a rough estimate of how the pH would change with acid addition. Due to the uncertainty of the solution volume introduced through many sequential pH measurements, the chloride binding in theses samples could not be accurately determined.

For chloride binding a separate set of 21 samples were acidified using the same steps as for the pH-samples, but the acidification was stopped at 7 different amounts of acid and thus different levels of pH. The acid volumes were 0.75, 2, 3.5, 7, 12, 14 and 18 mL. Triplet samples were stopped at each of these levels. After each sample triplet had their full amount of acid added, they were left for two weeks to equilibrate before analysis. The three samples with 14 mL acid were acidified further after pH and chloride measurements to a total volume of 22 mL acid to reach lower levels of pH. These samples were corrected for total solution volume and total mol chloride when calculating chloride binding (V_{tot} and n_{Cl} in Eq. (8), see Section 2.5). The NaCl-isotherm samples with 1.5 mol/L NaCl were used as reference samples for the HCl-samples and are called "0 mL" in the results (e.g. Figs. 7 and 11).

The samples with 15 g well-hydrated paste and 20 mL NaCl proved to have high capacity for buffering pH, preventing them from reaching a pH below 10.4. Additional HCl-samples were therefore prepared to study the effect of extreme acidification, with lower amounts of paste, thereby lowering the buffering capacity of the system. A set of three samples were prepared. They contained 10 g well-hydrated paste, 15 mL 1.5 mol/L NaCl, and had 4 mol/L HCl added in 10 steps of 2 mL for a total volume of 20 mL. These samples are named "10 g" to highlight the lower amount of hydrated paste, resulting in lower pH at the end.

2.3. Liquid analysis

The chloride concentrations and pH of all the samples were determined before proceeding with further experiments. For the HCl-samples, one of the three samples per acid volume was reserved for solid analysis, whilst one had its exposure solution analysed with inductively coupled plasma mass spectrometry (ICP-MS).

2.3.1. Chloride titration

The chloride concentrations in the samples were measured using a Titrando 905 titrator from Metrohm, with a 20 mL burette and 0.1 mol/L $AgNO_3$. After centrifuging the samples, a known sample volume between 0.2 and 1.0 mL depending on the expected chloride concentration was pipetted into a beaker. 20 mL deionized water, 1 mL of 1:10 diluted 65% HNO_3 (supplied by Merck) and 2.5 mL 0.2% polyvinyl alcohol (supplied by Merck) was then added to the beaker. The contents of the beaker were titrated to find the total molar amount of chloride, which was used to calculate the chloride concentration of the exposure solution at equilibrium ($C_{Cl,eq}$ in Table 2).

2.3.2. pH measurements

All pH measurements were conducted using a 6.0255.100 Profitrode from Metrohm at 20 °C. The electrode was calibrated daily with buffer solutions of pH 7, 10 and 13. The samples were first centrifuged to allow easier extraction of the exposure solution. To avoid contamination of the electrode from the cement paste, the measurement was performed by extracting 2 mL of the exposure solution into a separate 15 mL tube. The pH was measured in this tube, which allowed for the solution to fully cover the electrode. After being analysed the supernatant was poured back into the sample. The samples were weighed before and after each pH measurement, to keep track of the associated mass loss.

2.3.3. Inductively coupled plasma mass spectrometry

Samples for inductively coupled plasma mass spectrometry (ICP-MS) were prepared from the exposure solutions and from the wash-water from cold water extraction (see Section 2.4.1). The machine used for analysis was a Thermo Scientific Element 2 ICP-MS.

3–4 mL of the exposure solutions were extracted from each sample using 12 mL syringes, which were then deposited into small tubes through filters mounted on the tip of the syringes. 1 mL of the filtrated solutions were pipetted into 100 mL volumetric flasks, before being diluted to 100 mL with deionized water. 10 mL of these diluted solutions were pipetted into 15 mL centrifuge tubes, to which 140 µL 1:2 diluted 65% HNO_3 was added. This results in a 101.4 times dilution of the exposure solution with a 0.1 mol/L HNO_3-concentration.

All the ICP-MS samples were analysed for the concentrations of Al, Ca, Cl, Fe, K, Na, P, S and Si. Some elements like Al and Si were too close to the detection limit, preventing accurate quantification. These are therefore not included in Fig. 6. Although the Cl concentration was also analysed with ICP-MS, the concentrations from chloride titration were used to calculated chloride binding (see Section 2.5).

Table 2
pH, chloride concentration before chloride binding ($C_{Cl,free}$) and measured chloride concentration at equilibrium ($C_{Cl,eq}$) for the HCl-samples, with the NaCl and $CaCl_2$ isotherm samples. All samples had an initial sample mass of 15 g well-hydrated cement paste, except the sample with 10 g paste which is indicated with the star (*).

Sample	pH	$C_{Cl,free}$	$C_{Cl,eq}$
	[−]	[mol/L]	[mol/L]
1.5 mol/L NaCl	13.2	1.23	1.13
+0.75 mL HCl	12.9	1.32	1.21
+2 mL HCl	12.6	1.44	1.30
+3.5 mL HCl	12.3	1.58	1.41
+7 mL HCl	11.9	1.85	1.67
+12 mL HCl	11.9	2.12	1.95
+18 mL HCl	11.2	2.38	2.23
+22 mL HCl	10.4	2.55	2.41
+20 mL HCl (10 g paste)*	9.4*	2.67*	2.60*
0.25 mol/L NaCl	13.3	0.21	0.15
0.5 mol/L NaCl	13.3	0.42	0.34
1 mol/L NaCl	13.2	0.83	0.74
1.5 mol/L NaCl	13.2	1.23	1.13
2 mol/L NaCl	13.2	1.64	1.54
3 mol/L NaCl	13.1	2.45	2.33
0.25 mol/L $CaCl_2$	12.8	0.21	0.13
0.5 mol/L $CaCl_2$	12.5	0.43	0.29
1 mol/L $CaCl_2$	12.2	0.85	0.66
1.5 mol/L $CaCl_2$	12.1	1.28	1.05
2 mol/L $CaCl_2$	11.9	1.67	1.41
3 mol/L $CaCl_2$	11.7	2.52	2.21

2.4. Solid analysis

One sample from each triplet of the HCl-samples was used for solid analysis. The free water had to be removed from the wet cement paste before analysis, thereby stopping the hydration. Most of the exposure solution was removed by centrifuging the samples and extracting the supernatant with a pipette. Any excess solution containing chlorides had to be removed to prevent crystallization of chloride salts during the solvent exchange.

2.4.1. Cold water extraction and double solvent exchange

In order to analyse the solids, excess chloride solution had to be removed without precipitation of chloride salts. This was done by cold water extraction (CWE) [33], as described in the following paragraph.

After extracting most of the exposure solution, the contents of the sample tubes were homogenized with a spatula before 5 ± 0.001 g of the wet cement paste was placed together with 50 mL deionized water in a 250 mL beaker. The suspension was stirred for 3 min before it was filtrated, and the solids of each sample were then further treated with a

double solvent exchange.

For the double solvent exchange procedure, 100 mL isopropanol was added to the filtration unit with the solids. After stirring with a glass rod for 30 s, the suspension was left for 5 min before being filtrated. The walls of the filtration unit were rinsed with isopropanol during filtration. The isopropanol treatment was performed twice, before 20 mL petroleum ether was added to the filtration unit followed by 30 s stirring and 5 min rest before filtration until dry. The powder-like solids were stored overnight in a vacuum desiccator (−0.2 bar) before further analysis. Parts of the solids were cast in epoxy for SEM-EDS analysis. Another part was ground in a porcelain mortar to pass a 63 μm sieve. These ground solids were used for TGA, XRD and dissolved for ICP-MS analysis.

2.4.2. Thermogravimetric analysis

Thermogravimetric analysis (TGA) was used to investigate the changes in phase assemblage in the cement paste upon exposure, and to find the free water content of the well-hydrated cement paste. A Mettler Toledo TGA/DSC3+ was used to perform the experiments. All the methods included purging the chamber with N_2 at 50 mL/min. For each analysis, ca. 150 mg of the samples were placed into 600 μl alumina crucibles.

The free water content of the well-hydrated cement paste was found by drying non-chloride exposed cement paste at 40 °C until constant mass (10 h), before heating from 40 to 900 °C over 86 min at 10 °C/min. Parts of the same paste were, along with the chloride exposed samples, solvent exchanged, dried and ground. They were then also heated at 10 °C/min from 40 to 900 °C.

Decomposing phases can be identified as mass losses in specific temperature intervals [34]. C-S-H continually loses bound water between 40 and 600 °C, ettringite decomposes near 100 °C, hydrotalcite ($4MgO{\cdot}Al_2O_3\ 10H_2O$) near 350 °C and portlandite between 400 and 550°C. The AFm-phases Friedel's salt, monosulphate and monocarbonate have different decomposition peaks in the ranges of 150–200 °C and 250–400 °C. The mass% of bound water after exposure ($w_{\%}$) was determined as the mass loss between 40 and 550°C. The TGA-results are presented as mass loss (TG) and the derivative of the mass loss per (DTG) as functions of temperature, where the mass losses are normalized to the initial sample mass.

2.4.3. X-ray diffraction

Parts of the dry ground solids were analysed with X-ray diffraction (XRD) to identify crystalline phases. Approx. 0.5 g of the powders were front loaded into sample holders. They were then analysed in a Bruker AXS D8 Focus equipped with a Lynxeye detector, which was operating at 40 kV and 40 mA with CuKα radiation (wavelength of 1.54 Å). The scans ranged from 5 to 55°2θ using a step size of 0.01° 2θ and sampling time of 0.5 s per step. The XRD spectra were evaluated with the DIFFRAC.EVA V4.0 software from Bruker, the PDF4+ database from ICDD and the COD database.

2.4.4. Scanning electron microscopy

Parts of the unground samples were cast in epoxy and polished for SEM analyses. A Hitachi S-3400 N scanning electron microscope equipped with an EDS-detector from Oxford Instruments was used. EDS was performed with a working distance of 10 mm with a probe current of 75 μA and accelerating voltage of 15 kV. BSE images, EDS maps and point scans were acquired with a working distance of 10 mm. The elemental maps for Al, Cl, Si and Ca were used to select regions for point scan analyses. For each sample, 4 sites at 1000× magnification where scanned with 50 points at each site for a total of 200 points per sample. Half of the point scans were acquired from areas with high chloride and aluminium content, and the other half from areas of the cement paste matrix (high Si and Ca-content) to find the compositions of the AFm-phases and C-S-H respectively.

2.4.5. Quantifying paste dissolution

Eq. (9) shows that the calculated chloride binding depends on the total volume of free water in the sample. This volume is affected by the hydration and dissolution of the cement paste. If the cement paste hydrates, the volume of free water decreases and the calculated chloride binding increases. If the paste dissolves or its bound water content decreases the volume of free water increases, which leads to a decreased calculated chloride binding. A combination of ICP-MS and TGA were used to calculate the changes in the volume of free water in the cement paste, using similar methodology as Machner et al. utilized to quantify leaching [35].

All the chloride exposed pastes and the PC used to make the pastes were analysed using the ICP-MS, to study the amount of dissolved paste upon acid exposure. 50–300 mg of the dry powders (ground pastes and unhydrated PC) were dissolved in an UltraCLAVE Milestone high pressure digestion unit using 65% HNO_3. The dissolved samples were then checked for iron content using ICP-MS. Phases containing iron were assumed to not dissolve upon HCl exposure and could therefore be used to determine how much of the cement paste remained after exposure using Eq. (2).

$$Q_{r.p.} = \frac{m^1_{paste}}{m^0_{paste}} = \frac{m^0_{Fe}/m^0_{paste}}{m^1_{Fe}/m^1_{paste}} = \frac{Fe^0_{\%}}{Fe^1_{\%}} \tag{2}$$

Here $Q_{r.p.}$ is the fraction of the cement paste remaining after dissolution. The superscripts *0* and *1* refer to before and after chloride exposure respectively. m_{paste} is the mass of cement paste, m_{Fe} is the mass of iron and $Fe_{\%}$ is the mass% of iron in the cement paste. The ratios of m_{Fe}/m_{paste} are the results from the ICP-MS-dissolution experiments and are equivalent to $Fe_{\%}$. Assuming that the iron in the cement does not dissolve during acid exposure, m^0_{Fe} is equal to m^1_{Fe}. The fraction of remaining cement paste can therefore be expressed as the ratio between the mass% of Fe in the paste before and after exposure. Values for $Q_{r.p.}$, m_{paste} and $Fe_{\%}$ are given in Table 4.

The mass% of bound water and PC in the cement pastes were determined by TGA (see Section 2.4.2). Eq. (3) shows the relationship between the amount of paste, PC and bound water.

$$m_{paste} = m_{cement} + w = m_{paste}{\cdot}(mass\%_{cement} + w_{\%}) \tag{3}$$

Here m_{paste} is the mass of paste, m_{cement} is the mass of PC and w is the mass of bound water in the sample. $mass\%_{cement}$ is the mass% of PC and $w_{\%}$ is the mass% of bound water in the sample. Note that the sum of $mass\%_{cement}$ and $w_{\%}$ is 1 (or 100%). As described in Section 2.4.2, $w_{\%}$ is the mass loss from 40 to 550 °C in the TGA, and $mass\%_{cement}$ is therefore the remaining mass at 550 °C. With this relationship it is possible to relate the amount of iron in the cement paste to the amount of iron in the cement. Combining the results from the ICP-MS and TGA enabled finding the change in bound water content for the samples using Eq. (4).

$$\Delta w = w_0 - w_1 = m^0_{paste}{\cdot}w^0_{\%} - m^1_{paste}{\cdot}w^1_{\%} = m^0_{paste}{\cdot}(w^0_{\%} - Q_{r.p.}{\cdot}w^1_{\%}) \tag{4}$$

Here the sub/superscripts *0* and *1* indicate the hydrated cement paste before and after exposure respectively. Δw is the change in bound water for the cement paste, w is the mass of bound water, m_{paste} is the mass of cement paste in the sample, $w_{\%}$ is the mass% of bound water and $Q_{r.p.}$ is the fraction of remaining cement paste.

The change in bound water was found to only be a small portion of the total paste dissolution for the HCl-samples at low pH. When calculating the change in solution volume (see Section 2.5.1) the mass loss was therefore used instead of the change in bound water. Total mass loss from each sample was found using Eq. (5).

$$\Delta m_{paste} = m^0_{paste} - m^1_{paste} = m^0_{paste}{\cdot}(1 - Q_{r.p.}) \tag{5}$$

Here the sub/superscripts *0* and *1* indicate the cement paste before and after exposure respectively. Δm_{paste} is the change in mass of cement

paste, m_{paste} is the mass of cement paste and $Q_{r.p.}$ is the fraction of remaining cement paste found using Eq. (2). Values for $w_{\%}$, Δw and Δm_{paste} are given in Table 4.

2.4.6. Quantifying mass of portlandite

A quantification of the mass of portlandite in the samples was used to verify the validity of the thermodynamic model (see Section 2.6). The mass of cement paste changes upon acid exposure and the TGA yields the mass% of phases, which means the mass of CH has to be normalized. The mass loss associated with CH (between 400 and 550 °C) from the TGA was used in combination with the paste dissolution results to find the total mass of CH.

For a given sample, the mass% of CH in the cement paste was found using Eq. (6).

$$mass\%_{CH} = \frac{m_{CH}}{m_{paste}} = \frac{\Delta m_{400-550°C}}{m_{TGA}} \cdot \frac{M_{Ca(OH)_2}}{M_{H_2O}} \quad (6)$$

Here $mass\%_{CH}$ is the mass percentage of CH in the cement paste without free water, m_{CH} is the mass of CH in the paste and m_{paste} is the mass of cement paste without free water in each 50 mL sample tube. $\Delta m_{400-550\ °C}$ is the mass loss registered between 400 and 550 °C in the TGA of the solvent-exchanged cement paste (found using tangential integration of DTG-curves), m_{TGA} is the initial mass of the paste sample in the TGA, and $M_{Ca(OH)2}$ and M_{H2O} are the molar masses of CH (74 g/mol) and water (18 g/mol) respectively.

Using the mass% of portlandite, the mass of CH in each sample was found using Eq. (7).

$$m_{CH} = mass\%_{CH} \cdot m^1_{paste} = mass\%_{CH} \cdot m^0_{paste} \cdot Q_{r.p.} \quad (7)$$

Here the sub/superscripts *0* and *1* indicate the hydrated cement paste before and after exposure respectively. m_{CH} is the mass of portlandite in the sample in grams, given an initial 15 g well-hydrated cement paste. $mass\%_{CH}$ is the mass percentage of CH in the cement paste without free water, m_{paste} is the mass of cement paste without free water and $Q_{r.p.}$ is the fraction of the cement paste remaining after dissolution.

2.4.7. Quantifying changes to AFm

Changes in the total chloride binding are linked to the changes to the chloride-containing AFm-phases. Here a semi-quantification of the AFm was performed combining the results from TGA and ICP-MS. Assuming that the AFm-phase was a Friedel's salt solid solution, it was detected as a mass loss in the range 250–400 °C. Hydrotalcite also loses water in the same range, so the quantification is of the mass loss from both phases. It was assumed that hydrotalcite did not dissolve during exposure, as it has been demonstrated to be highly resistant to leaching [35]. This meant that there would be the same amount of hydrotalcite in all the samples, so that the changes in mass loss were due to changes in the AFm.

From the DTG-curves of all samples (see Figs. 7 and 8), the mass loss between 250 and 400 °C was calculated using the tangential integration method [34]. The mass losses (in mass% of the paste) were normalized to the amount of cement paste before exposure by multiplying with the remaining cement paste fraction $Q_{r.p.}$ (as described in Section 2.4.5).

2.5. Chloride binding

The hypothetical chloride concentration in the samples if there was no chloride binding ($C_{Cl,free}$) was calculated using Eq. (8), according to the equation from [36] modified to account for the additional water and chlorides added by the HCl.

$$C_{Cl,free} = \frac{(C_{NaCl/CaCl_2} \cdot V_{NaCl/CaCl_2}) + (C_{HCl} \cdot V_{HCl})}{V_{H_2O} + V_{NaCl/CaCl_2} + V_{HCl} + V_{paste}} = \frac{n_{Cl}}{V_{tot}} \quad (8)$$

Here $C_{NaCl/CaCl2}$ is the chloride concentration of the NaCl or $CaCl_2$ exposure solution (0.25, 0.5, 1, 1.5, 2 and 3 mol/L), $V_{NaCl/CaCl2}$ is the volume of the NaCl or $CaCl_2$ exposure solution (20 mL), C_{HCl} and V_{HCl} are the concentrations and volumes of the acid added to the sample (4 mol/L and between 0.75 and 22 mL respectively), whilst V_{H2O} is the volume of free water from the well-hydrated cement paste in each sample (found to be 4.3 mL per 15 g well-hydrated paste before exposure). This volume was determined by the mass loss of drying the non-exposed well-hydrated cement paste in a TGA at 40 °C until constant mass. V_{paste} is the solution volume from dissolution of paste (see Section 2.5.1), n_{Cl} is the total molar amount of chloride and V_{tot} is the total volume of the exposure solution in the sample.

Since the cement paste binds chlorides from the solution, the measured concentration at equilibrium will be lower than $C_{Cl,free}$. The difference between the measured chloride concentration ($C_{Cl,eq}$) and $C_{Cl,free}$ can be used to calculate the amount of chlorides bound by the cement paste. The chloride binding as g chloride per g dry cement paste ($N_{Cl,bound}$) was calculated using Eq. (9).

$$N_{Cl,bound} = \frac{M_{Cl} \cdot (C_{Cl,free} - C_{Cl,eq}) \cdot (V_{H_2O} + V_{NaCl/CaCl_2} + V_{HCl} + V_{paste})}{m_{sample} - m_{H_2O}} = \frac{M_{Cl} \cdot (n_{Cl} - C_{Cl,eq} \cdot V_{tot})}{m_{paste}} \quad (9)$$

Here M_{Cl} is the molar mass of Cl (35.453 g/mol), $C_{Cl,free}$ is the hypothetical chloride concentration in the sample in the absence of chloride binding (Eq. (8)), $C_{Cl,eq}$ is the measured equilibrium concentration of chlorides in the sample, m_{sample} is the amount of well-hydrated cement paste in the sample (15 g) and m_{H2O} is the mass of free water in the paste, as determined by drying at 40 °C in a TGA until constant mass (4.3 g per 15 g paste). As described in Eq. (1), the difference between the mass of well-hydrated paste and the mass of free water is the mass of cement paste, m_{paste}.

2.5.1. Accounting for paste dissolution and solution volume increase

One of the main differences between the present study and previous chloride binding studies was accounting for the increase of solution volume due to dissolution of cement paste. The volume increase must be incorporated in Eqs. (8) and (9) by the additional factor V_{paste} in the total volume V_{tot}. Eq. (10) shows the calculation of V_{tot} and Eq. (11) shows the calculation of V_{paste}.

We were unable to directly determine the volume increase from paste dissolution, therefore the mass loss of cement paste was divided by two different densities to find the upper and lower limits for the change in volume. The upper limit was found by assuming that the paste dissolved into solution with an approximate density of 2 g/mL, to represent a density in between that of the exposure solution and the cement paste. The lower volume limit was found assuming a density of 3 g/mL, corresponding to the cement paste dissolving into a liquid with approximately the same density and volume as the solid cement paste.

$$V_{tot} = V_{H_2O} + V_{NaCl/CaCl_2} + V_{HCl} + V_{paste} \quad (10)$$

$$V_{paste} = \frac{\Delta m_{paste}}{\rho} = \frac{m^0_{paste} - m^1_{paste}}{\rho} = \frac{m^0_{paste} \cdot (1 - Q_{r.p.})}{\rho} \quad (11)$$

Here V_{tot} is the total volume of the exposure solution in the sample, V_{H2O} is the volume of free water from the well-hydrated cement paste, $V_{NaCl/CaCl2}$ is the volume of the NaCl or $CaCl_2$ exposure solution, V_{HCl} is the volume of the acid added to the sample and V_{paste} is the solution volume from dissolution of paste. The superscripts *0* and *1* indicate the hydrated cement paste before and after exposure respectively. m_{paste} is the mass of cement paste, Δm_{paste} is the change in mass of cement paste from Eq. (5), and $Q_{r.p.}$ is the fraction of remaining cement paste found using Eq. (2). ρ is the density of the liquid the paste dissolves into (2 or 3 g/mL used as models). Values for $Q_{r.p.}$, m_{paste} and Δm_{paste} can be found in Table 4. Fig. 17 shows the calculated values for V_{paste} for both ρ = 2 and 3 g/mL. For the other volumes in Eq. (10), see Eq. (8).

2.6. Thermodynamic model

The Gibbs free energy minimization software for Geochemical Modelling (GEMS) [37–39] was used to model the changes in the hydrate phase assemblage and in the liquid phase composition in the samples upon acidification with 4 mol/L HCl or exposure to various concentrations of NaCl/$CaCl_2$ at 20 °C. A cement-specific database (CEMDATA14) containing solubility products of cementitious materials was used in combination with the PSI-GEMS database. The CSHQ-model for C-S-H proposed by Kulik was used [40]. The XRF-results of the PC was used as input for the PC composition in the model. The model assumed a 70% degree of reaction. Several phases were blocked in the model to prevent it from predicting the formation of phases that are kinetically impossible at the conditions of the exposure: gibbsite, kaolinite, thaumasite, hematite, magnetite, brucite and quartz. Siliceous Fe-hydrogarnet was enabled, whilst siliceous Al-Fe-hydrogarnet was blocked. An amount of Al equal to 0.05 mol Al/mol Si in C-S-H was removed to account for the Al-uptake of C-S-H, thereby predicting more realistic amounts of AFm phases. Norwegian cements are rich in magnesium, which mostly occur as unreactive periclase. Previous hydration studies on similar cements have therefore either neglected Mg [16,35] or blocked hydrotalcite from forming [29,36]. In this study 50% of the Mg in the system was forced to form periclase to reduce the reactivity of Mg. This also reduces the formation of hydrotalcite, which would otherwise consume most of the aluminium and reduce the amount of AFm.

3. Results

3.1. Thermodynamic model

Fig. 4 shows the volumes of the phases present in the samples upon exposure to increasing amounts of HCl, as predicted by the thermodynamic model. The dashed lines indicate the amounts of acid added to the samples in this study. According to the model, portlandite is the first phase to start dissolving when HCl is added. No other phase is predicted to start dissolving whilst CH is still present in the sample. CH buffers the pH of the system, resisting the lowering of the pH caused by the addition of acid. The C-S-H starts to decompose once all the portlandite has dissolved at 12 mL acid. It will continue to gradually dissolve in the range of 12 to 33 mL acid. Ettringite remains stable until 24 mL acid is added, after which it dissolves. Friedel's salt starts dissolving at 20 mL acid. A series of phases appear to form at high acid volumes, including gypsum, natrolite and amorphous silica.

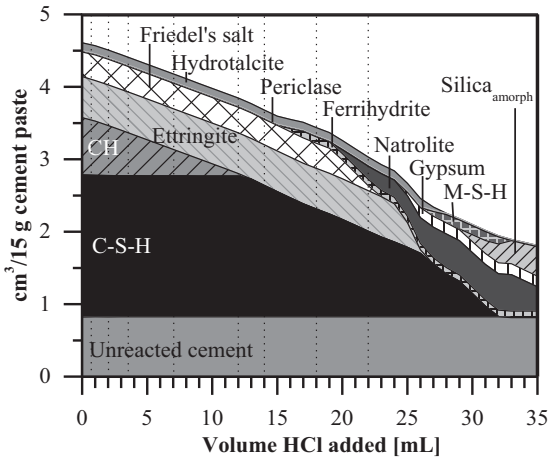

Fig. 4. The volumes of solid phases present in the HCl-samples for different volumes of 4 mol/L HCl added to the cement paste, as predicted by the thermodynamic model. Each dashed line indicates the volume of acid added to one of the samples.

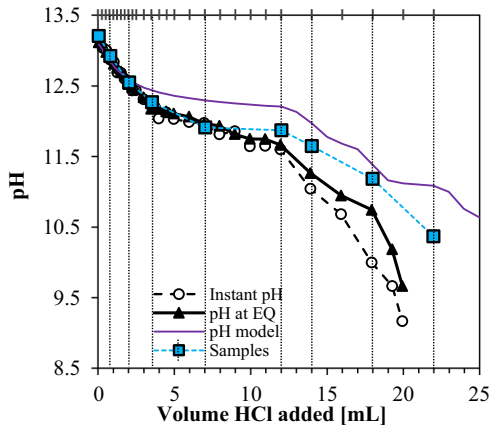

Fig. 5. The gradual decrease of the pH in the exposure solution of the HCl-samples as increasing volumes of acid was added, from experimental results and the thermodynamic model. "Instant pH" and "pH at EQ" refer to measuring the pH 5–10 min and 1 day after acid addition respectively. The vertical lines indicate the levels of acid additions for the acid exposure samples.

3.2. Exposure solution

3.2.1. pH and acid volume

Fig. 5 shows how increasing volumes of acid added to the HCl-samples changed the pH of the exposure solution. The tick marks on the top show the acidification steps, and the vertical lines show the intended acid volumes for the HCl-samples. Blue boxes show the measured pH of the HCl-samples. "Instant pH" and "pH at EQ" refer to the progression samples (see Section 2.2), and respectively are results from measuring the pH 5–10 min and 1 day after acid addition. The development of the pH of the pore solution as predicted by the thermodynamic model is also included ("pH model"). The measured pH decreased almost linearly between 0 and 4 mL acid, before changing to a less steep slope between 4 and 12 mL acid. The slope becomes steeper again after 12 mL acid. The thermodynamic model fits the experimental data well below 4 mL acid but overestimates the pH above 4 mL. It does however follow a similar progression with an initial rapid decline (0–4 mL), followed by a plateau (4–12 mL), before the rapid decline commences at 12 mL acid.

The samples used for pH progression quickly reached equilibrium after acid was added, as can be seen from the small differences between the pH at 5–10 min and 1 day after acid additions. The difference between the curves increased as the acid dosage was increased to 2 mL and the buffer capacity was lowered due to dissolution of hydrates. Each pH measurement removed some of the exposure solution, approximately 8.5 mL in total across 54 measurements per sample. This reduced the buffering capacity of the sample, thus the pH in the progression samples decreased faster than the HCl-samples. The overall trends were however still similar.

3.2.2. Elemental concentrations in the pore solution

Fig. 6 shows the concentrations of Ca, K, S, Na and Fe in the exposure solution of the HCl-samples as a function of the measured chloride concentration, both measured with ICP-MS and as predicted by the thermodynamic model. The model for Fe is not included, as it predicts concentrations 3–4 orders of magnitude lower than the experimental results. The overall changes are accurately predicted by the model. The concentrations of Cl and Ca gradually increase, whilst the concentration of K steadily decreases. For S, the model shows a similar progression as the experimental results with an initial sharp decrease. At approximately 2.5 mol/L chloride the model and experimental results show an increased S concentration. It is important to note here that the experiments and model show similar results but likely for different reasons. The model predicts the dissolution of ettringite,

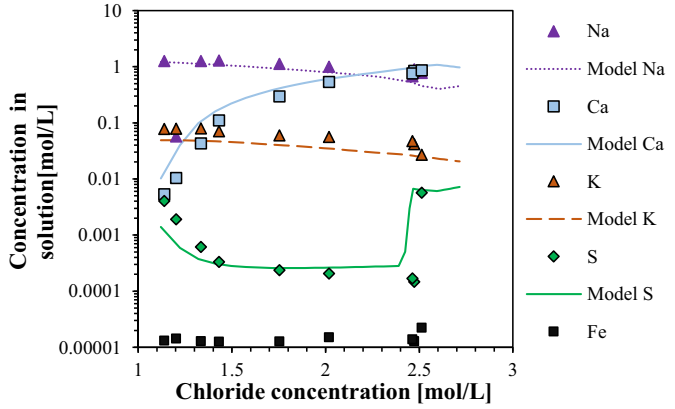

Fig. 6. The concentrations of Na, Ca, K, S and Fe in the exposure solution in the HCl-samples, as functions of the volume of 4 mol/L HCl added. The symbols are experimental results from ICP-MS whilst the lines are from the thermodynamic model.

increasing the concentration of S. The XRD, TGA and SEM-EDS of the solid phases show instead that ettringite is still present in the last sample, perhaps even to a larger extent than in the other samples (see Figs. 7, 11 and 14). The concentration of Fe remained close to constant in the range. As stated in Section 2.3.3, the chloride concentration measured using titration was used to calculated chloride binding, although there was a good correlation between ICP-MS and titration (R^2 = 0.97, see additional uploaded data).

3.2.3. Chloride concentration and pH of exposure samples

The chloride binding in the samples depends on the difference between the expected and measured chloride concentrations and changes in solution volume. As the change in volume requires incorporating the results from the dissolution experiments (see Section 3.3.4), we will first present the results relating to the chloride concentration. The contributions of chloride concentration and volume change on chloride binding will be discussed in Section 4.1.

Table 2 gives the pH and measured chloride concentrations ($C_{Cl,eq}$, from chloride titration) in the HCl-samples and the NaCl/$CaCl_2$ isotherm samples, along with the calculated chloride concentration before chloride binding ($C_{Cl,free}$, Eq. (8)). The pH for the NaCl isotherm samples were almost constant, only dropping from 13.3 to 13.1 from 0.25 to 3 mol/L NaCl. $CaCl_2$ and HCl-exposure both lead to reduced pH, respectively dropping from 12.8 to 11.7 and from 13.2 to 9.4. The expected chloride concentration increased with increasing concentration and volume of the added solution.

3.3. Changes in phase assemblage

We investigated the phase assemblage in the samples with a multi-method approach consisting of XRD, TGA, SEM-EDS and paste dissolution combined with ICP-MS. The combination of TGA and XRD enables the identification of the hydrates present in the samples and detection of changes in the relative amounts of hydrates. SEM-EDS provides images of the microstructure and information on the composition of the phases present. The dissolution-ICP-MS-experiment allowed quantification of cement paste dissolution and change in solution volume.

3.3.1. Thermogravimetric analysis

Drying the non-exposed paste at 40 °C for 10 h resulted in a loss of 29 mass%, and the mass loss of the dried paste between 40 and 550 °C whilst heating at 10 °C/min yielded a bound water of 21 mass% (meaning 21 mass% of the 71 mass% remaining after drying). The cement paste therefore had a total water content of 44 mass%, equalling a total w/c-ratio of 0.78. Percentage of bound water in the cement pastes are provided in Table 4. There was a general trend of increasing mass% of bound water with increasing chloride concentration in the exposure solution.

Fig. 7a) shows the mass loss curves (TG) and the first derivative of those curves (DTG) for the cement paste in the HCl-samples and non-exposed paste, as determined by TGA. The ettringite mass loss for the 10 g paste sample appears to be larger than for the other samples. Fig. 7b) presents the DTG-curves in the temperature interval from 250 to 500 °C, highlighting the mass loss peaks for Friedel's salt and hydrotalcite (275–375 °C). From 0 to 18 mL acid there was a trend of gradually increasing peak size for both peaks. The peak at approximately 310 °C decreased in size from 18 to 22 mL and appears to vanish almost completely for the extreme acidification sample (10 g).

Fig. 8 shows the same curves as in Fig. 7 but for the NaCl and $CaCl_2$ isotherm samples. The samples have similar DTG-curves, where the main differences are in the portlandite and Friedel's salt/hydrotalcite-peaks. Fig. 8b) shows that the size of the FS/Htc-peaks increased with increasing chloride concentration, much more so for $CaCl_2$ than NaCl. The increased peak size for the NaCl isotherm samples is mostly in the higher temperature peak (350 °C), whilst for $CaCl_2$ the increase is in the lower temperature peak (310 °C).

Fig. 9 shows the amounts of portlandite in the samples calculated with Eq. (7), in grams total per sample. The HCl-samples show a rapid decrease in portlandite, dropping from 1.1 g at 1.1 mol/L Cl to 0 g at 2.2 mol/L Cl. The NaCl isotherm samples show little change in the amount of portlandite, remaining near 1.1 g. The $CaCl_2$ isotherm samples show a decrease from 1.2 to 1.0 g CH from 1.1 to 2.2 mol/L Cl. Comparing the experimental results with the thermodynamic model, the predicted values from the model are at all points larger for NaCl and

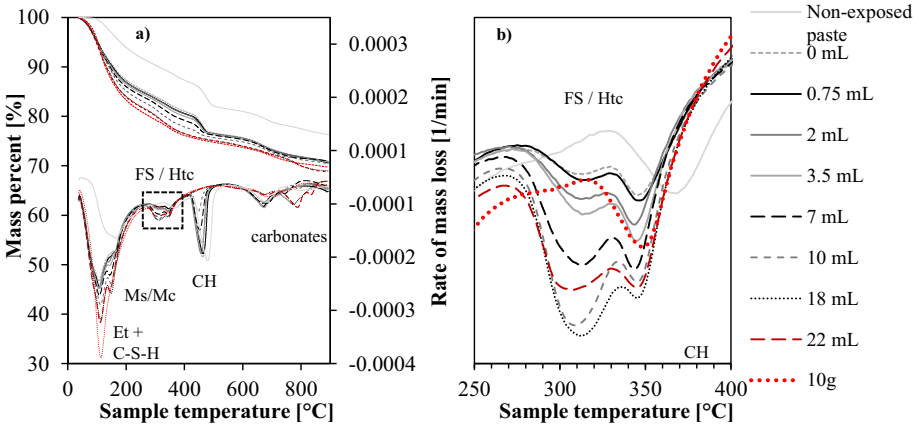

Fig. 7. TG (a, top) and DTG (a, bottom) curves from the HCl-samples. b) shows a selected part of the DTG-curves between 250 and 450 °C, focused on the mass loss peaks related to Friedel's salt and hydrotalcite. Characteristic peaks for ettringite and C-S-H (Et + C-S-H), monosulphate/monocarbonate (Ms/Mc), Friedel's salt/hydrotalcite (FS/Htc), portlandite (CH) and carbonate phases are indicated.

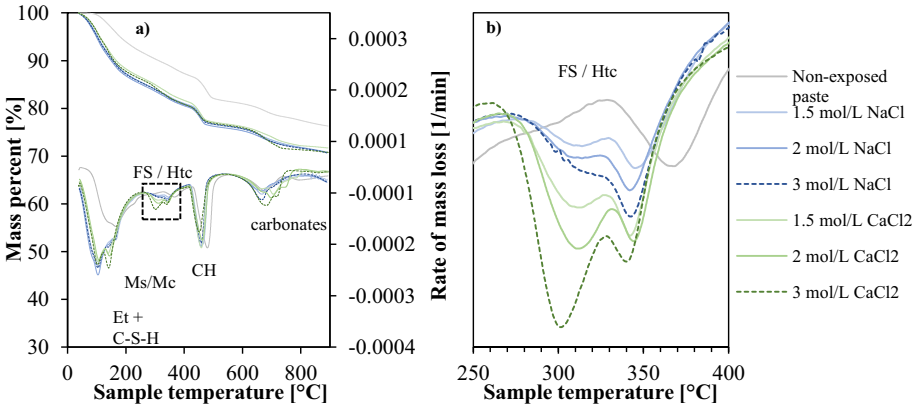

Fig. 8. TG (a, top) and DTG (a, bottom) curves from the NaCl and $CaCl_2$ isotherm samples. b) shows a selected part of the DTG-curves between 250 and 450 °C, focused on the mass loss peaks related to Friedel's salt and hydrotalcite. Characteristic peaks for ettringite and C-S-H (Et + C-S-H), monosulphate/monocarbonate (Ms/Mc), Friedel's salt/hydrotalcite (FS/Htc), portlandite (CH) and carbonate phases are indicated.

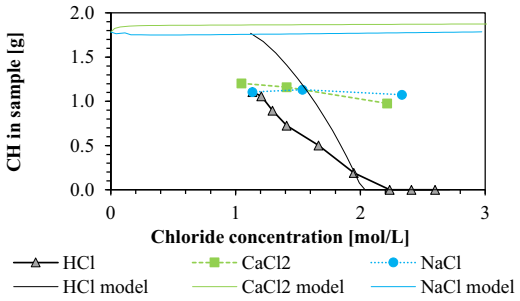

Fig. 9. Quantification of portlandite (CH) in the samples after exposure, as functions of the chloride concentration in the exposure solution for the HCl-samples, and the NaCl and $CaCl_2$ isotherm samples. The same values from the thermodynamic model are also included.

$CaCl_2$, and it fails to model the decrease in CH for the $CaCl_2$ isotherm samples. The model does however predict similar decreased CH-content for the HCl exposure as the experimental results. It appears that the model does not predict the phase assemblage in the paste completely, but it captures the main trends of change during exposure.

Fig. 10 shows how the mass loss from the Friedel's salt solid solution and hydrotalcite (between 250 and 400 °C) for the samples changes with increasing chloride concentration. The mass loss was found by integrating the area of the mass loss peak in the DTG-curves and was normalized to the mass of cement paste before exposure. The $CaCl_2$ and NaCl isotherm samples showed increased mass loss with increasing chloride exposure, with the former showing a higher initial value and increased more than the latter. They respectively increased from around 0.7 to 1.3 and 0.4 to 0.6 mass%. The HCl-samples showed an increase in mass loss from around 1 to 2.3 mol/L chloride, increasing the mass loss from 0.4 to 1.0 mass%. Above 2.3 mol/L the mass loss

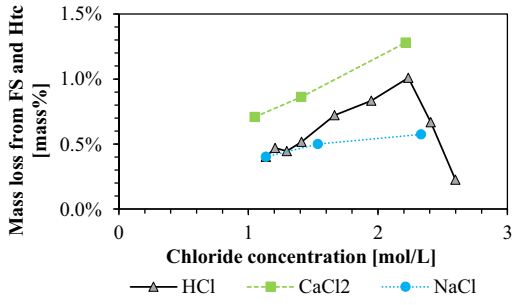

Fig. 10. Quantification of the mass loss peaks for Friedel's salt and hydrotalcite (FS and Htc) in mass% normalized to the mass of cement paste before exposure, as functions of the chloride concentration in the exposure solution for the HCl-samples, and the NaCl and $CaCl_2$ isotherm samples.

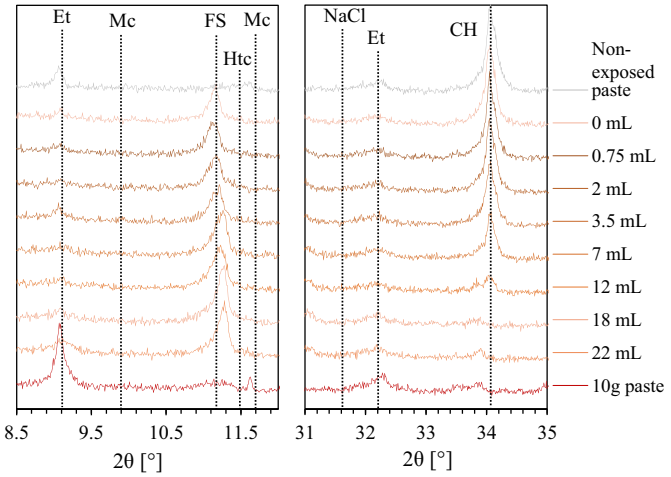

Fig. 11. XRD spectra of the HCl-samples with indications of reflection peaks for ettringite (Et), monocarbonate (Mc), Friedel's salt (FS), hydrotalcite (Htc) NaCl and portlandite (CH).

decreased to 0.3 mass% at 2.6 mol/L.

3.3.2. X-ray diffraction

Fig. 11 shows the XRD spectra of the HCl-samples. For the HCl-samples clear reflections are visible for Friedel's salt (11.19° 2θ) and portlandite (18.09° 2θ). Clear reflection peaks for ettringite (9.08° 2θ) appear only in the non-exposed cement paste and in the harshly leached sample with only 10 g cement paste. Small humps are however still visible for the other samples, indicating that some poorly crystalline ettringite was present. The peaks of portlandite decreased as more acid was added, before completely disappearing above 18 mL acid. This agrees very well with the TGA results. No reflections for NaCl were observed in any of the samples, indicating that the CWE was successful in removing excess exposure solution and therefore preventing the precipitation of NaCl in the samples upon drying. The (001)-reflection of Friedel's salt shifts to higher angles for higher acid volumes. The reflection for Friedel's salt is greatly reduced for the extreme acidification sample (10 g), to the point of almost disappearing.

Fig. 12 shows the same XRD spectra as Fig. 11 but for the NaCl and $CaCl_2$ isotherm samples. The AFm-peaks in the $CaCl_2$-samples are all at higher angles than for NaCl.

3.3.3. Scanning electron microscopy

SEM-EDS was used to study the composition of the chloride binding phases in the cement pastes. The results of the point analyses are presented and described in this section as molar ratios of various elements in scatter plots. Each point in EDS scatter plots is acquired from a

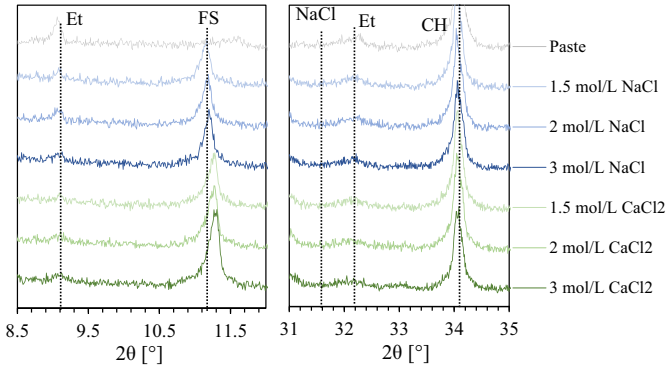

Fig. 12. XRD spectra of the NaCl and $CaCl_2$ isotherm samples with indications of reflection peaks for ettringite (Et), Friedel's salt (FS), NaCl and portlandite (CH).

volume of the cement paste, which contains a mix of different phases. The points will therefore lie between the ideal compositions (expressed in molar ratios) of the intermixed phases.

In the elemental maps obtained by SEM-EDS, all samples showed clear distinct areas with high chloride content, which were likely high in chloride-containing AFm-phases. Fig. 13a) shows the atomic ratios of Cl/Ca from the point analyses plotted as a function of the Al/Ca-ratio for the HCl-samples with 0 and 22 mL acid added. The compositions of Friedel's salt (FS), Kuzel's salt (Kuzel), carbonate and hydroxyl-AFm (C/OH AFm) and C-S-H are indicated. Most of the points are clumped together in the bottom left, and are from regions of mainly C-S-H. The rest of the points trend towards the composition of the AFm-phases,

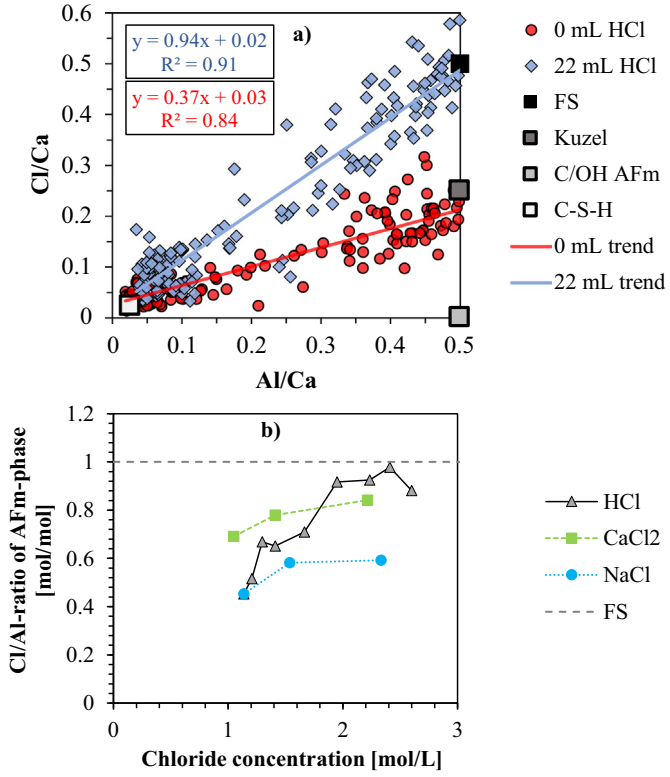

Fig. 13. SEM-EDS point analyses of the samples in this study. Subfigure a) shows the atomic Cl/Ca-ratios of the samples with the least (0 mL) and the most (22 mL) acid along with a linear regression fitting of the data. Subfigure b) shows the Cl/Al-ratio for the regression lines of a Cl/Si – Al/Si-plot from each of the samples, found using the least squares method. The compositions of Friedel's salt (FS), Kuzel's salt (Kuzel, $3CaO{\cdot}Al_2O_3{\cdot}(CaCl_2)_{0.5}{\cdot}(CaSO_4)_{0.5}{\cdot}11H_2O$) and monocarbonate/hydroxyl AFm (C/OH AFm) are also indicated.

indicated with the regression lines found using the least squares method.

Fig. 13a) illustrates with regression lines for the point analyses the composition of the AFm-phases. We are interested in the atomic Cl/Al-ratios of the AFm to see potential changes in the solid solution upon exposure. The plot in Fig. 13a) is useful for illustrating the principle of how to observe changes in AFm composition, but it has the disadvantage of normalizing to calcium which is leached during acid exposure. Rather than using the Cl/Al-ratio normalized to Ca it is possible to find the Cl/Al-ratio by normalizing to an element which is independent to the AFm, for instance Si. All EDS point analyses from the samples were plotted in individual graphs (one per sample) with the Cl/Si-ratio as functions of the Al/Si-ratio, and regression lines were found. The slopes of these lines were used as estimates for the Cl/Al-ratio in the AFm, and these Cl/Al-ratios are presented in Fig. 13b) as functions of the chloride concentration. These plots have largely varying scales for the axes and as such they cannot be nicely plotted in the same figure (individual Cl/Si vs Al/Si-plots are provided in the additional uploaded data). The NaCl and $CaCl_2$ isotherm samples show a small increase in Cl/Al-ratio as the chloride concentration increased from 1 to 1.5 mol/L, after which they level out. The increase is from approximately 0.45 to 0.59 Cl/Al and from 0.69 to 0.84 for NaCl and $CaCl_2$ respectively. The HCl-samples show a trend of increasing Cl/Al-ratio with increasing chloride concentration, from 0.45 to a maximum value of 0.98. This is approaching the stoichiometric composition of Friedel's salt with a Cl/Al-ratio of 1, as indicated in the figure. Similar results with these methods have been shown by Sui et al. [41].

Fig. 14 shows the most relevant EDS-results for sulphur in the samples. Subfigure a) shows the atomic S/Ca-ratio in the point analyses from the HCl-sample exposed to 0.75 mL acid, as a function of the Al/Ca-ratio. Compositions of the C-S-H, ettringite, monosulphate (Ms), Kuzel's salt and Friedel's salt or carbonate/hydroxyl AFm (FS, C/OH AFm) are indicated. This type of plot is conventionally used to demonstrate the presence of sulphate-containing AFm phases, ettringite or a mixture of these. The results from this sample are representative of the other HCl-samples above pH 10, in that no trend towards monosulphate or Kuzel's salt were observed. At this scale and with these axes it is near impossible to determine if there are small amounts of these sulphate phases intermixed with the C-S-H. The plot does however clearly show that there is an AFm-phase present which does not contain sulphate, like Friedel's salt or carbonate AFm.

To more closely examine which phases are intermixed with the C-S-H, Fig. 14b) and c) shows the atomic S/Si-ratios of three samples (0 mL and 3.5 mL HCl plus the sample with 10 g paste) as functions of the Ca/Si-ratio. These two plots show the same data but with different sizes for the axes to highlight different parts of the results.

In both plots, all points lie along or to the right of lines with a slope of S/Ca = 0.5. This corresponds to the S/Ca-ratio that is typical for ettringite. Ettringite is the phase with the highest S/Ca ratio in this cement paste system, thereby the line with a slope of 0.5 acts as an upper limit for the S/Ca ratio. The scatter in the points towards the right side of the line is due to different levels of intermixing of ettringite with other phases. When increasing the size of the axes, subfigure c) shows that the only sample with points of high S/Si ratios is from the 10 g paste sample. In the elemental maps (provided as additional data) there were clear areas with a high sulphur content from which these point scans were gathered. The points measured in these areas fall on the ettringite-line in Fig. 14c), which indicates that these were areas containing mainly ettringite with little to no other phases intermixed. It is reasonable to assume that these pockets of ettringite formed due to precipitation, possibly formed by the excess S in solution reacting with the Al released from dissolving AFm.

In the same figures, one can also obtain information regarding the composition of the C-S-H. In subfigure b) the points which are near the composition of the C-S-H are highlighted with the black ellipse. Because C-S-H has the lowest Ca/Si-ratio of the present phases, the leftmost

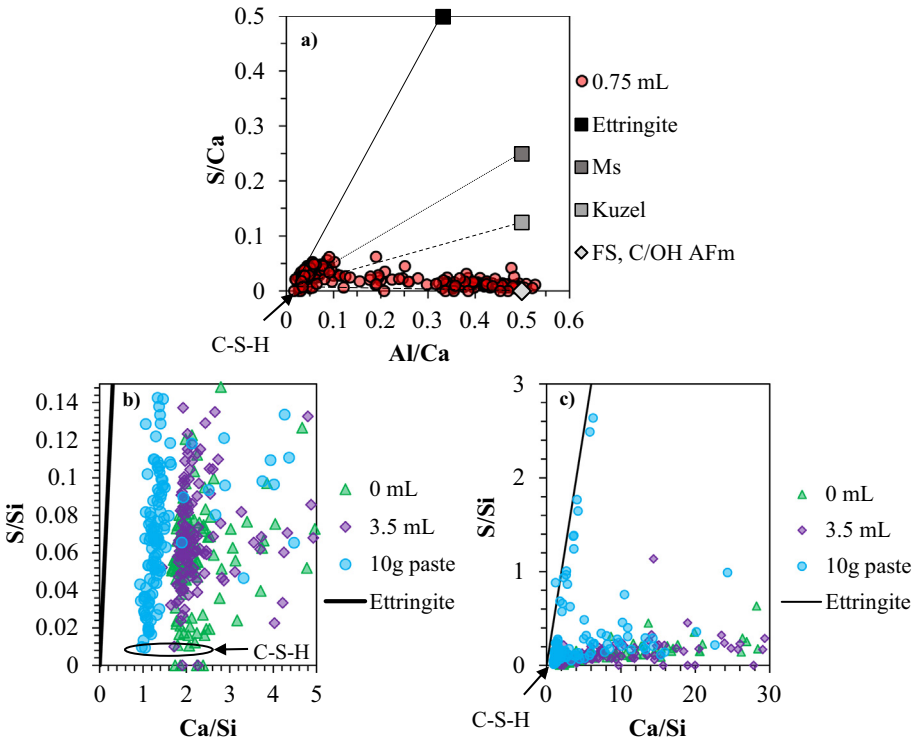

Fig. 14. Subfigure a) shows atomic S/Ca-ratios as a function of the Al/Ca-ratio for the EDS point analyses from the sample exposed to 0.75 mL 4 mol/L HCl, with indications for the compositions of the C-S-H, ettringite, monosulphate (Ms), Kuzel's salt and Friedel's salt/carbonate or hydroxyl AFm (FS, C/OH AFm). Subfigures b) and c) show the atomic S/Si-ratios of three samples (0 mL and 3.5 mL HCl plus the sample with 10 g paste) as functions of the Ca/Si-ratio. b) and c) show the same data but with different sizes for the axes. The black line indicates the S/Ca-ratio of ettringite, which is 0.5.

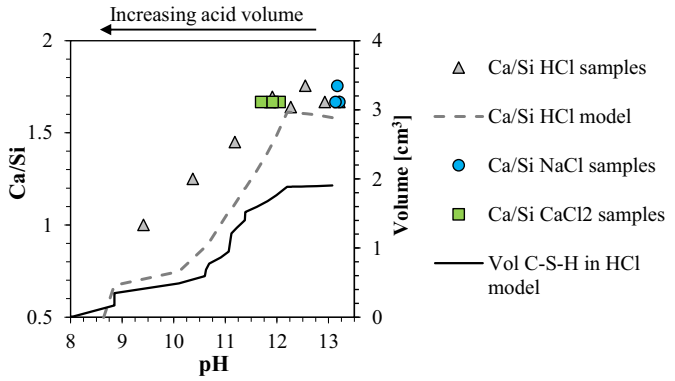

Fig. 15. Atomic ratios of Ca/Si from EDS for the C-S-H phases in the HCl-samples, NaCl and $CaCl_2$ isotherm samples, presented as functions of the pH of the exposure solution. The same ratio of Ca/Si for the HCl-samples and the volume of C-S-H from the thermodynamic model are also included.

boundary of the cloud of points indicates the Ca/Si-ratio of the C-S-H. The points from the 10 g paste sample are found to the left of the points from the 0 and 3.5 mL samples, which agrees with the lower Ca/Si-ratios of the 10 g sample compared to the others as shown in Fig. 15. The lower boundary of the cloud of points is also likely to be close to the S/Si-ratio of pure C-S-H, since other phases contain less Si or more S. For the 0 mL HCl and 10 g paste samples the S/Si-ratio of the C-S-H appears to be around 0.01, whilst for the 3.5 mL sample it is closer to 0.02 indicating a higher sulphate adsorption. This could coincide with the lowered S concentration in Fig. 6 when going from 0 to 3.5 mL acid. Similar plots for the other samples (provided in additional uploaded data) show that the lower boundary of the point cloud decreases when the amount of acid is higher than 3.5 mL indicating lower S adsorption. However, this does not correlate with the S concentration in the solution (see Fig. 6), which does not increase with the supposed decreasing S adsorption on the C-S-H. The concentration measurements therefore do not agree with this interpretation of S adsorption using the SEM-EDS data, and further study is needed to explain these discrepancies.

The Ca/Si-ratio of the C-S-H in the samples was found using the method described by Scrivener et al. [42], and Fig. 15 shows how the Ca/Si-ratios for the HCl-samples changed with the pH of the exposure solution. Also included in Fig. 15 is the Ca/Si-ratio and volume of C-S-H as predicted by the thermodynamic model. For the samples with 12 mL or less acid there was no clear trend with only small fluctuations in the Ca/Si-ratio (± 0.1). After 18 mL acid the ratio drops from 1.7 to 1.5, further dropping to 1.4 at 22 mL acid. The model predicts a small increase in the ratio for a pH drop from 13 to 12.2, before it steadily decreases down to 0.7 at a pH of 8.8. The model predicts a lower Ca/Si-ratio than the experimental results, especially as the pH decreases to 11.

The chloride content of the C-S-H in the samples were approximated following the methods described by Scrivener et al. [43], which were also used by De Weerdt et al. [12,13,29] and Sui et al. [41], to see if the results were comparable with those from the aforementioned studies. Estimates for the atomic Si/Ca, Al/Ca and Cl/Ca-ratios can be found using Figs. 13 and 16. Fig. 16 shows the atomic Cl/Ca-ratios of the point analyses from the HCl-samples with 0 and 22 mL acid, as functions of the atomic Si/Ca-ratios. Table 3 shows the estimated atomic ratios, and

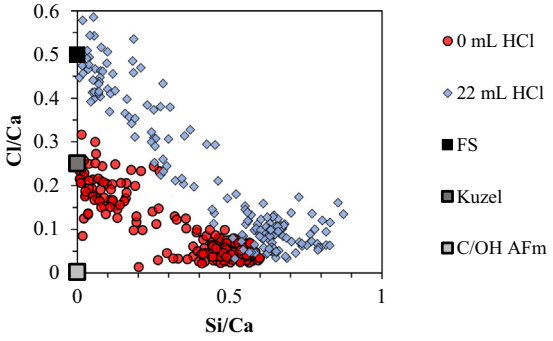

Fig. 16. Atomic ratios of Cl/Ca plotted as function of the Si/Ca-ratio for the EDS point analyses from the samples exposed to 0 and 22 mL 4 mol/L HCl. Compositions for Friedel's salt (FS), Kuzel's salt (Kuzel) and carbonate/hydroxyl AFm (C/OH AFm) are indicated.

Table 3
Atomic Si/Ca, Al/Ca and Cl/Ca-ratios of the C-S-H in the HCl-samples with 0 and 22 mL acid added. The results from the present study are compared to those from Sui et al. [41] studying OPC-pastes exposed to 0.5 mol/L NaCl.

Sample	Si/Ca	Al/Ca	Cl/Ca
1.5 mol/L NaCl	0.6	0.03	0.03
+22 mL HCl	0.8	0.05	0.04
0.5 mol/L NaCl [41]	0.54 ± 0.04	0.054 ± 0.03	0.038 ± 0.059
3 mol/L NaCl	0.6	0.03	0.05
3 mol/L NaCl [29]	0.6	0.05	0.10
3 mol/L $CaCl_2$	0.5	0.03	0.07
3 mol/L $CaCl_2$ [29]	0.5	0.05	0.15

for 1.5 mol/L NaCl with no acid they are comparable to [29,41]. The 22 mL acid sample has a higher Si/Ca-ratio due to the decalcification of the C-S-H, which could also be the reason for the increased Cl/Ca-ratio. $CaCl_2$-exposure increases the amount of calcium, lowering the Si/Ca-ratio. The differences between the Cl/Ca-ratios of the NaCl and $CaCl_2$ isotherm samples from the present study and those from [29] are most likely caused by the CWE-procedure removing excess chlorides from the paste, thereby reducing the amount of Cl precipitating after solvent exchange. The C-S-H in the HCl-samples was also leached of Ca, thereby naturally increasing the Si/Ca, Al/Ca and Cl/Ca-ratios.

3.3.4. Dissolution of cement paste

The changes in iron content determined by the ICP-MS dissolution experiments (see Section 2.4.5) enabled quantifying the dissolution of cement paste. Table 4 shows the measured pH, Fe-content of the cement pastes and the measured bound water content from the TGA. These were used to calculate the fraction of remaining cement after exposure ($Q_{r.p.}$), mass of cement paste after exposure (m_{paste}), change in bound water (Δw) and the mass of dissolved paste for each sample relative to the initial mass of paste (Δm_{paste}). Using the Fe-content ($Fe_{\%}$) of the paste to quantify dissolution appears to work well considering that the concentration of Fe remained near constant during acid exposure (see Fig. 6). With increasing additions of acid, the mass% of Fe increased, indicating more dissolution of the cement paste. The NaCl and $CaCl_2$ isotherm samples showed a trend of decreasing mass% Fe, and likely had more hydrates form at higher chloride concentrations. Most samples also showed an increased mass% of bound water ($w_{\%}$) compared to the cement paste before exposure, which could indicate further hydration after exposure or that parts of the unreacted cement have dissolved. As mentioned in Section 2.4.5, the change in bound water was much smaller than the mass of dissolved paste in the HCl-samples with 2 or more mL acid. The NaCl and $CaCl_2$ isotherm samples and the HCl-samples above pH 10.4 have negative Δw, which means they have a larger mass of bound water after exposure even when accounting for dissolution of paste.

Table 4
Measured pH, iron-content ($Fe_{\%}$ as mg Fe/g cement paste, from ICP-MS) and bound water ($w_{\%}$, from TGA) with calculated fraction of non-dissolved cement ($Q_{r.p.}$), mass of cement pastes after exposure (m_{paste}), released bound water after exposure (Δw) and mass of dissolved paste. The paste masses, change in bound water and dissolved paste are per sample, where all samples started with 15 g well-hydrated cement paste. The only exception is the 10 g-sample, indicated with the star (*).

Sample	pH	$Fe_{\%}$	$w_{\%}$	$Q_{r.p.}$	m_{paste}	Δw	Δm_{paste}
	[-]	[mg/g]	[%]	[%]	[g]	[g]	[g]
Cement	–	18.8	–	–	–	–	–
Cement paste before exposure	–	15.5	18.5	100%	10.7	–	–
1.5 mol/L NaCl	13.2	16.5	23.8	94%	10.1	−0.41	0.64
+0.75 mL HCl	12.9	16.4	24.1	95%	10.1	−0.46	0.57
+2 mL HCl	12.6	18.1	23.9	86%	9.2	−0.21	1.53
+3.5 mL HCl	12.3	18.7	24.1	83%	8.9	−0.16	1.82
+7 mL HCl	11.9	18.4	24.2	84%	9.0	−0.20	1.70
+12 mL HCl	11.9	19.1	24.7	81%	8.7	−0.17	2.01
+18 mL HCl	11.2	19.6	25.4	79%	8.5	−0.17	2.22
+22 mL HCl	10.4	23.2	25.4	67%	7.2	0.17	3.56
+20 mL HCl (10 g paste*)	9.4*	25.1*	25.7*	62%*	4.4*	0.19*	2.73*
1.5 mol/L NaCl	13.2	16.5	23.8	94%	10.1	−0.41	0.64
2 mol/L NaCl	13.2	16.1	24.2	96%	10.3	−0.52	0.38
3 mol/L NaCl	13.1	15.6	23.7	100%	10.7	−0.54	0.05
1.5 mol/L $CaCl_2$	12.1	15.8	23.3	98%	10.5	−0.47	0.18
2 mol/L $CaCl_2$	11.9	15.4	23.2	101%	10.8	−0.52	−0.06
3 mol/L $CaCl_2$	11.7	14.9	23.5	104%	11.1	−0.63	−0.41

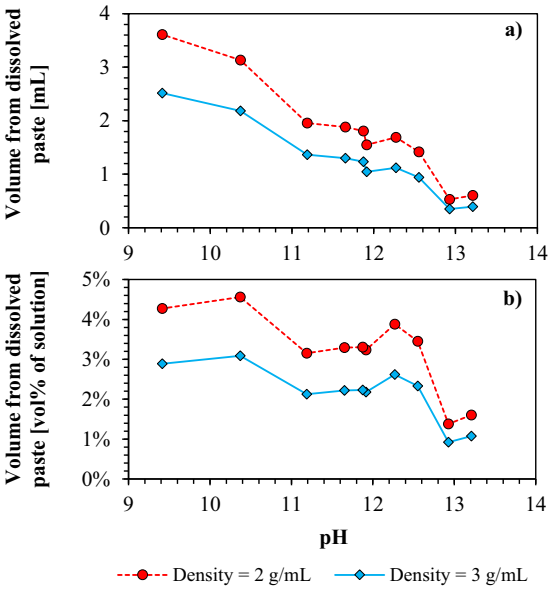

Fig. 17. The calculated increase in solution volume for the HCl-samples using the experimental mass loss of cement paste and two models for the density of the dissolved paste. Subfigure a) gives the total volume increase per sample (V_{paste} in Eq. (11)) given 15 g well-hydrated paste, and subfigure b) gives the volume increase as a percentage of the total solution volume.

With the mass of dissolved paste, two estimates for changes in solution volume from dissolving cement paste (V_{paste}) were made as described in Section 2.5.1 and Eqs. (10) and (11). The densities used to convert from grams paste to mL solution were 2 and 3 g/mL. This gave a range of values near which the real volume was likely to be found. Fig. 17 shows the calculated increases in solution volume caused by paste dissolution in the HCl-samples, as a function of the pH in the solution. The increases are given as mL per sample given 15 g well-hydrated cement paste and an initial 20 mL 1.5 mol/L NaCl solution (a), and as percentage of the total solution volume (b). The total volume of solution in each sample was calculated with Eq. (10), where V_{H2O} was 4.3 mL, $V_{NaCl/CaCl2}$ was 20 mL and V_{HCl} ranged from 0 to 22 mL. For all models the volume gradually increased as the pH fell. Higher densities meant lower volume, thus the 3 g/mL estimate was lower than 2 g/mL. In absolute units the volume increase ranged from 0.3 to 1.6 mL for the 3 g/mL model and from 0.4 to 2.5 for the 2 g/mL model. In terms of volume percentage, they varied between 0.9 to 3.1 vol% and 1.4 to 4.5 vol%.

4. Discussion

The results of this study and their potential impact will be discussed in three parts. First the effect of paste dissolution and HCl on the total chloride binding of Portland cement paste will be discussed. Then, the mechanisms behind changes in binding will be illuminated, focusing on the AFm-phases. Finally, the results will be compared with an experimental chloride profile to link the present study to field observations.

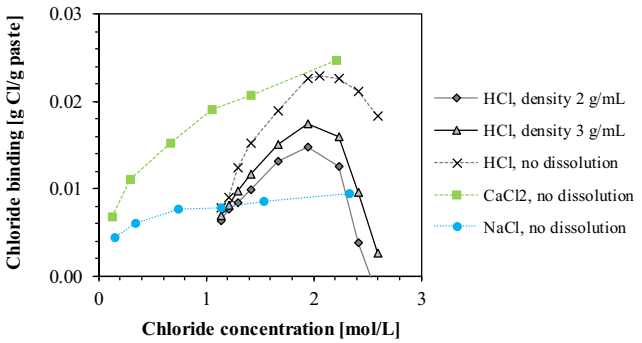

Fig. 18. Chloride binding of the HCl-samples and NaCl and $CaCl_2$-isotherm samples as functions of the measured chloride concentration in the exposure solution. The NaCl and $CaCl_2$-isotherm samples show values calculated assuming no cement paste dissolution and solution volume change. The HCl-samples show chloride binding values assuming three different changes in volume resulting from paste dissolution: No dissolution or volume change (black crosses), and dissolution of paste into liquid with density 3 g/mL (grey triangles) or 2 g/mL (grey diamonds).

4.1. Total chloride binding

4.1.1. Determining increase of solution volume

Before being able to calculate the effect of HCl on the chloride binding in cement paste, the question of paste dissolution and solution volume increase must be solved. Using the calculated volume increases in Fig. 17, three different levels of chloride binding can be found for the HCl-samples: One for each density (2 and 3 g/mL), plus one where the dissolution is not accounted for, i.e. with zero volume change. Fig. 18 shows these three levels of chloride binding for the HCl-samples, compared with the chloride binding isotherms for the NaCl and $CaCl_2$ isotherm samples. These were all calculated using Eq. (9), with the chloride concentrations provided in Table 2 and solution volume changes in Fig. 17.

The first thing to note is that the chloride binding isotherms for NaCl and $CaCl_2$ are very similar to previous studies [24,27–30]. NaCl shows a small gradual increase with increasing chloride concentration, almost plateauing at high concentrations. $CaCl_2$ shows a rapid increase in binding at lower concentrations, before beginning to level out but still increasing more than for NaCl. In comparison to the HCl-samples, the NaCl and $CaCl_2$ isotherm samples have much smaller changes in paste mass and therefore exposure solution volume (see Table 4). Thus, the correction for paste dissolution has a smaller impact on the calculated chloride binding for the NaCl and $CaCl_2$ isotherm samples than for the HCl-samples. The effect is however still present and might be worth taking into consideration in future chloride binding studies.

Fig. 18 demonstrates the impact of paste dissolution and the change in solution volume for artificial leaching with HCl. Depending on how the volume change is calculated, the chloride binding after HCl-exposure can be slightly larger than NaCl, similar to $CaCl_2$, or somewhere in between. Before progressing the discussion, some of these models must be ruled out and discarded. The present results demonstrate that the dissolution of paste has a tremendous effect on the calculation of chloride binding. In our previous study [16] we calculated without accounting for dissolution and the results were therefore similar to those of "HCl, no dissolution" in Fig. 18. This assumption appears to have oversimplified the problem considering the large percentage of dissolved paste in Table 4, and the model should be discarded. This leaves using the densities of 2 or 3 g/mL for the dissolving cement paste. Using 2 g/mL yields negative binding values, which suggests that it is not close to the real density. The same conclusion is supported by comparing the mass change in bound water and dissolved paste in Table 4. If most of the mass loss could be attributed to change in bound water, the density of the dissolving paste would be closer to the density

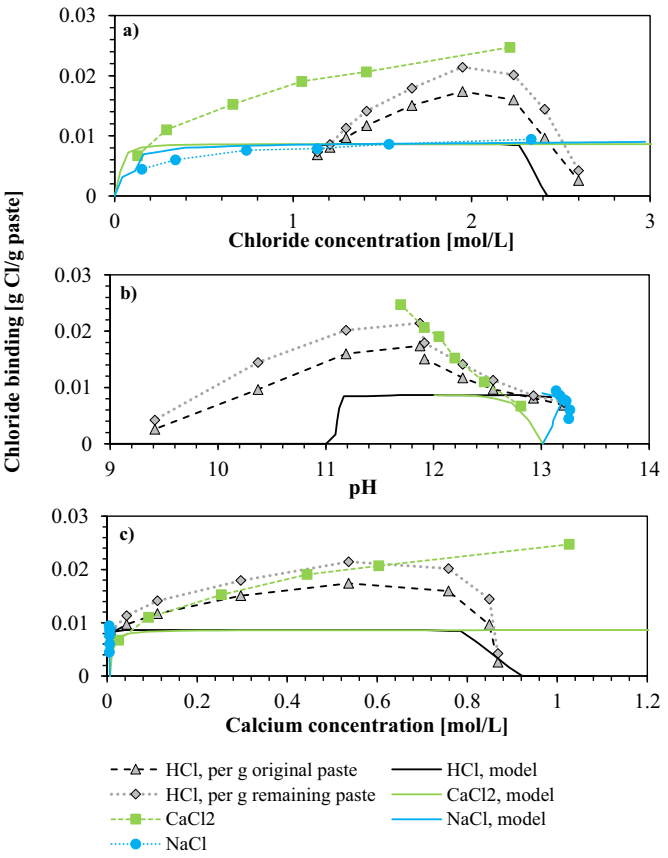

Fig. 19. Chloride binding of the HCl-samples, together with the NaCl and $CaCl_2$-isotherm samples. The binding of the HCl-samples has been calculated using the assumption of the cement paste dissolving into liquid with a density of 3 g/mL. For the HCl-samples, the chloride binding has been normalized to the mass of cement paste in the sample before exposure ("per g original paste") and the mass of the remaining cement paste after exposure ("per g remaining paste"). Also included are the chloride binding values predicted by the thermodynamic model (indicated "model" in the legend). Subfigure a) shows the values as functions of the measured chloride concentration, subfigure b) as functions of the pH, and subfigure c) as functions of the calcium concentration in the exposure solution.

of water than that of the cement paste. However, the loss of bound water is negative and an order of magnitude lower than the mass of dissolved cement paste for most of the HCl-samples. Since the mass loss of paste is not caused by loss of bound water (see Δw in Table 4), it stands to reason that the dissolving parts are anhydrous components of the paste. This means the paste dissolves into a liquid with a density closer to that of the cement paste than that of water. Thus, using 3 g/mL is a better approximation for the density and thereby the increase in solution volume. Moving forward with the discussion this 3 g/mL value will be used to compare the chloride binding of HCl with that of NaCl and $CaCl_2$. It must still be noted that this is only an estimate for the volume, as we could not measure it directly.

4.1.2. The effect of HCl on chloride binding in cement paste

With more realistic values for the experimentally determined chloride binding in the HCl-samples, they can now be compared to the binding isotherms for NaCl, $CaCl_2$ and the values predicted by the thermodynamic model. Fig. 19 shows the chloride binding for all these different samples and models, as functions of the chloride concentration (a), pH (b) and calcium concentration (c) in the exposure solution. The binding in the HCl-samples has been normalized to the masses of cement paste before and after exposure, labelled "per g original paste" and "per g remaining paste" respectively. Since there is less paste after

exposure, the latter has consistently higher chloride binding values than the former. Since the NaCl and $CaCl_2$ isotherms have smaller changes in amount of paste before and after chloride exposure, the two different normalizations would be almost identical. The normalizations to remaining cement paste are therefore not included in this figure.

Considering first Fig. 19a), it is very clear that the addition of HCl increases the chloride binding of the cement paste drastically compared to NaCl. Below 2 mol/L chloride the binding increases rapidly, doubling the values of the NaCl isotherm at the same concentration. Above 2 mol/L, the chloride binding starts to decrease. It appears to decline slowly at first, before plummeting towards zero near 2.6 mol/L. Exposure to small volumes of HCl improves the ability of the cement paste to bind chlorides, whilst larger volumes prove detrimental to chloride binding. The changes in chloride binding caused by adding HCl compared to NaCl are very unlikely to be related to increased chloride concentration, but rather the increasing in calcium concentration or decrease in pH.

Fig. 19b) and c) shows that comparing the chloride binding of the HCl-samples to the binding isotherms for NaCl and $CaCl_2$ relative to the chloride concentration can be deceiving. It appears from the outset that $CaCl_2$ yields larger chloride binding than HCl in similar conditions, but this is not necessarily the case. Comparing the $CaCl_2$ samples to the HCl samples normalized to the remaining paste shows that they have almost identical levels of chloride binding at similar pH and calcium concentration. For both sample sets the binding continues to increase as the pH drops from around 13 to 12. Only below pH 12 does the binding decrease for the HCl-samples, whilst the $CaCl_2$-samples do not reach such a low pH.

When considering the chloride binding as a function of the calcium concentration in the exposure solution, Fig. 19c) shows that the HCl-samples can show comparable chloride binding as the $CaCl_2$-samples. The two sample sets show similar trends from 0 to 0.6 mol/L Ca, above which the binding for the HCl-samples decreases whilst the $CaCl_2$-isothem increases. As with the chloride concentration, the increased calcium concentration is unlikely to cause the decrease in chloride binding of the HCl-samples, which is rather caused by the decreased pH.

The thermodynamic models are unable to accurately predict the experimental chloride binding, which is mostly due to the model not accounting for physical binding by C-S-H. It will only account for chloride binding in stoichiometric Friedel's salt. The model does however agree with the experimental data when it comes to the eventual decrease in chloride binding. This is due to the dissolution of Friedel's salt at low pH, which is a process well suited for thermodynamic modelling. The experimental chloride binding values are the sum of the chemical binding by AFm and the physical binding by C-S-H. Before the mechanisms behind the increase and eventual decrease can be determined, a closer examination of the AFm-phases must be carried out.

4.2. Mechanisms of pH influencing chloride binding

The chloride binding by the AFm-phases is mainly determined by two factors. The first is the amount of AFm, as more AFm means more possible binding. The second is the Cl-content of the phases, which can be expressed as mol Cl/mol AFm, or as mol Cl/mol Al. Possible adsorption on AFm is ignored here since it is likely a minor contribution. Considering the gradual changes in the molar Cl/Al-ratio (see Fig. 13) it is safe to assume the AFm is a solid solution between Friedel's salt and either carbonate or hydroxyl AFm. The gradual change is also likely the cause of the shift in reflection peak near 11.2° 2θ for the HCl-samples, as seen in Fig. 11.

Fig. 13b) shows that the Cl/Al-ratio of the AFm-phases increases with increasing chloride concentration for all the samples. Fig. 10 shows that the amount of chloride-containing AFm also increases, except for the HCl-samples above 2.3 mol/L chloride. Fig. 20 shows the mass losses from Fig. 10 and the Cl/Al-ratios from Fig. 13 as functions of the pH.

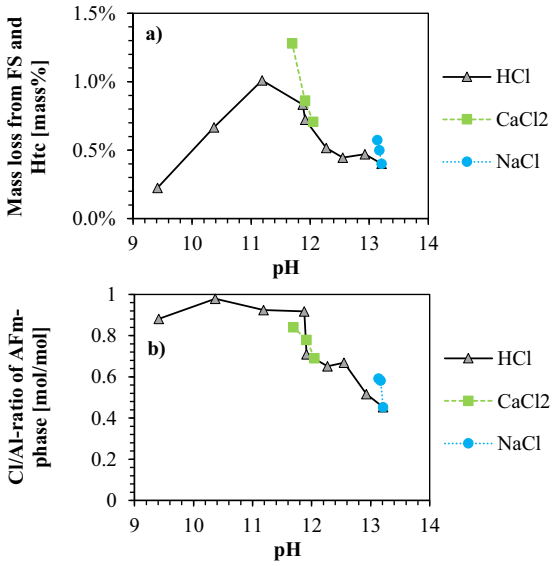

Fig. 20. Mass loss from Friedel's salt solid solution (FS) and hydrotalcite (Htc) (a) and atomic Cl/Al-ratio of the AFm in the samples (b) both as functions of the pH in the exposure solution.

For both HCl and $CaCl_2$ the increased chloride binding as the pH decreases from 13 to 12 is linked to the increased chemical binding by the AFm. It has previously been shown that the increase in Ca-concentration from adding $CaCl_2$ could lead to formation of additional AFm [27]. The present study shows that the same can occur without introducing extra calcium to the system, but rather by liberating calcium as the pH is lowered and portlandite dissolves. Although the source of Al required to form the additional AFm was not conclusively determined, it might have originated from the C-S-H or from the AFt. In the case of NaCl, no large change in AFm-content is observed, coinciding with little to no changes in the calcium concentration or pH. The mechanisms driving the increased chloride binding during HCl and $CaCl_2$-exposure appear to be similar, with the exception that the HCl-samples reach a higher Cl/Al-ratio than the $CaCl_2$-isotherm samples. The total increased chloride binding is likely a combination of the proven increase in chemical binding and increased physical binding by C-S-H, although the exact contribution of each could not be accurately determined.

The progression of changes to the mass of AFm closely matches that of the total chloride binding when comparing Figs. 19b) and 20a). HCl and $CaCl_2$ show similar progressions, and the eventual decline in the HCl-samples at low pH is present in both figs. A key difference is that whilst the amount of AFm only decreases below pH 11, the total chloride binding flattens our or decreases below pH 12. Fig. 20b) shows that there appears to be a good correlation between the Cl/Al-ratio of AFm and the pH in the pore solution. Since the chloride content of the AFm increases with decreasing pH from 13.2 to 10.4 (see Fig. 20b), the decreased chloride binding must be caused by reduced physical binding. It can therefore be concluded that as the pH drops below 12, the ability of C-S-H to bind chlorides is reduced. The chemical chloride binding by AFm is reduced at some point below pH 11, due to the dissolution of AFm but not a reduction in Cl/Al-ratio.

4.3. Relation to leaching in field studies

With an idea of the interplay between pH and chloride binding the results from this study can be compared to field studies of concrete exposed to sea water. Sea water leaching reduces the pH in the concrete and a zonation of different phases appear at varying depths from the exposed surface [12–14]. The artificial leaching with HCl does not fully represent real leaching, as there is no transport of ions in or out of the

system. For instance, none of the HCl-samples show any signs of forming the Mg-rich phases observed in the outer millimetre of field samples [13]. The HCl-sample at lowest pH does however show an apparent increase in ettringite content, which coincides with an increased S concentration in the solution. For this sample much of the AFm has dissolved, releasing aluminium into solution which could precipitate as ettringite. Since no significant amounts of monosulphate or Kuzel's salt were detected, additional S released into solution is most likely to have been previously adsorbed on C-S-H. Lower Ca/Si-ratio should indeed cause the adsorption of sulphate to decrease [44], however this was only observed in the 10 g paste sample and not the other samples with reduced Ca/Si-ratio (18 and 22 mL HCl, see Fig. 15). As mentioned in Section 3.3.3, the appearance of the ettringite as large pockets with little to no other phases intermixed indicates that there was significant precipitation of ettringite after the harsh acid exposure.

If the cement paste before exposure represents the bulk paste deep inside a sea water exposed concrete, the gradual decreasing pH of the HCl-samples represent moving outwards to the surface where the pH decreases due to leaching. Considering the apparent precipitation of ettringite at low pH, it can be imagined that the HCl-sample at lowest pH was able to simulate the leaching at a depth of 0.5–2 mm from the surface. This is where an ettringite-rich layer is formed in sea water exposed concrete according to [13]. A depth of 20 mm corresponds to how deep CH-leaching is observed in the same study, so the HCl-samples could be thought of as simulating leaching from a depth of 20 mm going outwards to the surface with increasing amounts of acid and lower pH.

Fig. 21 gives an idea of how these results influence future interpretations of experimental chloride profiles. The experimental chloride profile from NaCl-exposure, adapted from [9] (see Fig. 1) are plotted alongside the measured pH and chloride binding of the HCl-samples. With no experimental depth in the present study to directly compare, the pH and Cl-binding values have been assigned hypothetical depths so that the shape of the pH-curve is similar to that of the portlandite-leaching in [9]. This comparison will here be used to illustrate the potential impact of the present study.

Comparing the chloride profile, pH and chloride binding in Fig. 21, they can be divided into four separate regions labelled I-IV. Beginning at the surface, section I is where severe leaching causes a drop in pH to some point below 12. This corresponds to the HCl-samples where the chloride binding is reduced below the maximum, going towards zero at low pH. The outermost layer of exposed concrete will likely have little

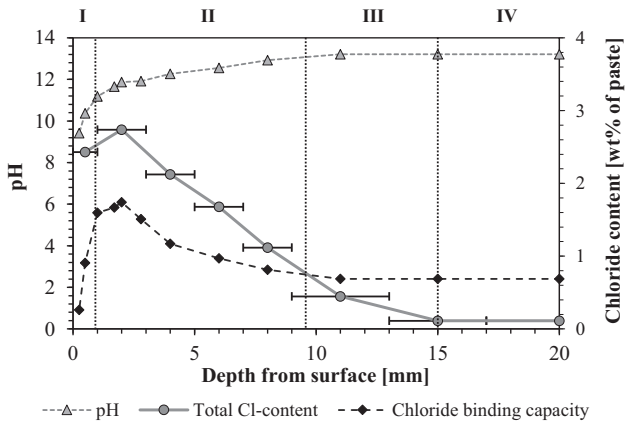

Fig. 21. Total chloride content from De Weerdt et al. [9] normalized to paste (water + binder, circles) as a function of depth from surface exposed to NaCl. The horizontal bars indicate the depth intervals the mortar was ground into. Also included are the values for pH (triangles) and chloride binding (diamonds) from the present study, adapted to the depth based on the leaching of CH in [9]. Four different regions corresponding to important changes in pH and chloride binding are indicated, labelled I-IV.

to no chloride binding. The chloride profile shows that the chloride content is still quite large in this section, because it is wide enough to include depths where there is still significant chloride binding.

Section II starts where the peak of the chloride profile is observed. In field studies this is where the pH has been reduced so that the cement paste can bind larger amounts of chlorides. The peak corresponds to the HCl-samples near pH 12 which showed the largest chloride binding. Going towards the surface the pH is reduced too much, dissolving AFm and altering the physical binding by C-S-H, and going inwards increases the pH which again reduces the chloride binding by lowering the Cl/Al-ratio of the AFm and the amount of AFm formed.

In sections I and II there are more chlorides present than can be bound by the cement paste. This changes in section III, which starts at the point where the total chloride content becomes lower than the chloride binding capacity of the cement paste. In section III and inwards it is possible that little to no chloride will be free in solution. Finally, section IV represents the bulk paste, where little to no effect of leaching or chloride ingress can be detected. Note that the results from the HCl-samples have been extended to illustrate this, meaning the pH and chloride binding of the points at 12, 15 and 20 mm are all from the 1.5 mol/L NaCl-sample.

5. Conclusion

This study has investigated how the pH in the pore solution influences the chloride binding of Portland cement pastes. Cement paste samples were exposed to NaCl, $CaCl_2$ and HCl solutions. Chloride binding isotherms were determined for NaCl and $CaCl_2$ exposure. The pH was lowered by exposing the paste to NaCl before gradually adding HCl. The chloride binding of the cement paste exposed to HCl was calculated using chloride titration and accounting for dissolution of paste using ICP-MS.

As the pH decreased from 13 to 12 upon HCl addition the chloride binding increased greatly compared to NaCl, approaching the chloride binding of $CaCl_2$-exposure. When the pH fell below 12 the chloride binding decreased significantly, approaching zero at pH 9.

Increasing chloride binding from pH 13 to 12 was linked to both increasing amounts of chloride-containing AFm solid solution and increasing Cl/Al-ratio of the AFm. Below pH 12 the amount of AFm decreased due to dissolution. The exact influence of C-S-H on changes to chloride binding could not be determined, but it has some effect since the total chloride binding decreases before the AFm starts to dissolve. Low pH will cause reduced chloride binding near the surface of sea-water exposed concrete.

Comparing the chloride binding of the HCl-samples with experimental chloride profiles from submerged chloride-exposed mortar gives insight into the cause of the peaking behaviour. The peak likely occurs at a depth where leaching reduces the pH to a value close to 12. This increases the chloride binding of the cement paste, thereby increasing the total chloride content. Closer to the exposed surface the paste suffers harsher leaching, reducing the chloride binding and total chloride content. The combination of lower binding in the outer section and increased binding in the following section causes the peaking behaviour in chloride profiles.

CRediT authorship contribution statement

Petter Hemstad: Conceptualization, Methodology, Validation, Investigation, Data curation, Writing - original draft, Writing - review & editing, Visualization, Project administration. **Alisa Machner:** Conceptualization, Methodology, Writing - review & editing. **Klaartje De Weerdt:** Conceptualization, Methodology, Writing - review & editing, Supervision, Funding acquisition.

Declaration of competing interest

The authors declare that they have no known competing financial interests or personal relationships that could have appeared to influence the work reported in this paper.

Acknowledgements

The authors would like to thank Barbra Lothenbach, Gilles Plusquellec and Tone Østnor for helpful discussions. We would also like to thank the anonymous reviewers for their critical and constructive comments. Additional thanks go to Oda Tjetland for assistance with sample preparation and titration, Syverin Lierhagen for performing the ICP-MS-measurements and to Arild Monsøy for preparing polished sections for the SEM.

Appendix A. Portlandite quantification

Table 5
Data for from TGA used for quantification of portlandite. m_{TGA} is the mass of the cement paste placed in the TGA crucible, $\Delta m_{400–550\ °C}$ is the mass loss from CH found by integrating the DTG-peak (given as both mg and mass%), $mass\%_{CH}$ is the mass% of CH in the cement paste after exposure, m_{CH} is the mass of portlandite in each sample given 15 g well hydrated cement paste before exposure. Also included are the measured mass losses between 400 and 550 °C as mass% of the cement paste after exposure and the mass% of CH calculated using the aforementioned mass loss instead of $\Delta m_{400–550\ °C}$.

Sample	m_{TGA}	$\Delta m_{400–550\ °C}$		$mass\%_{CH}$	m_{CH}	Mass loss from 400 to 500 °C	Mass% CH from total mass loss
	[mg]	[mg]	[mass%]	[mass%]	[g]	[mass%]	[mass%]
1.5 mol/L NaCl	96.08	2.57	2.67	11.00	1.11	4.83	19.84
+0.75 mL HCl	102.76	2.61	2.54	10.44	1.06	4.66	19.16
+2 mL HCl	82.55	1.96	2.37	9.76	0.90	4.42	18.19
+3.5 mL HCl	101.10	2.01	1.99	8.17	0.73	4.08	16.78
+7 mL HCl	94.31	1.28	1.36	5.58	0.50	3.41	14.01
+12 mL HCl	111.00	0.59	0.53	2.19	0.19	2.60	10.67
+18 mL HCl	101.20	0.00	0.00	0.00	0.00	1.95	0.00
+22 mL HCl	89.15	0.00	0.00	0.00	0.00	1.92	0.00
+20 mL HCl (10 g paste)	93.24	0.00	0.00	0.00	0.00	1.89	0.00
1.5 mol/L NaCl	96.08	2.57	2.67	11.00	1.11	4.83	19.84
2 mol/L NaCl	79.19	2.11	2.66	10.95	1.13	4.64	19.07
3 mol/L NaCl	83.22	2.04	2.45	10.08	1.07	4.54	18.68
1.5 mol/L $CaCl_2$	80.59	2.24	2.78	11.43	1.20	4.98	20.49
2 mol/L $CaCl_2$	102.60	2.69	2.62	10.78	1.16	4.90	20.13
3 mol/L $CaCl_2$	78.63	1.68	2.14	8.78	0.98	4.40	18.08

References

[1] U. Angst, B. Elsener, C.K. Larsen, Ø. Vennesland, Critical chloride content in reinforced concrete — a review, Cem. Concr. Res. 39 (2009) 1122–1138.
[2] K. Tuuti, Corrosion of Steel in Concrete, PhD, Stockholm, Sweden (1982).
[3] International Federation for Structural concrete, fib, Model code for concrete structures 2010, Ernst & Sohn, Berlin, Germany, 2013.
[4] L.O. Nilsson, E. Poulsen, P. Sandberg, H. Sørensen, O. Klinghoffer, HETEK, chloride penetration into concrete, state-of-the-art, Transport Processes, Corrosion Initiation, Test Methods and Prediction Models, 1996.
[5] Model Code for Service Life Design: Model Code, International Federation for Structural Concrete, Lausanne, Switzerland, 2006.
[6] M.R. Geiker, E.P. Nielsen, D. Herfort, Prediction of chloride ingress and binding in cement paste, Mater. Struct. 40 (2007) 405–417.
[7] I. Galan, F.P. Glasser, Chloride in cement, Adv. Cem. Res. 27 (2015) 63–97.
[8] M.K. Moradllo, S. Sadati, M. Shekarchi, Quantifying maximum phenomenon in chloride ion profiles and its influence on service-life prediction of concrete structures exposed to seawater tidal zone – a field oriented study, Constr. Build. Mater. 180 (2018) 109–116.
[9] K. De Weerdt, B. Lothenbach, M.R. Geiker, Comparing chloride ingress from sea water and NaCl solution in Portland cement mortar, Cem. Concr. Res. 115 (2019) 80–89.
[10] E.P. Nielsen, M.R. Geiker, Chloride diffusion in partially saturated cementitious material, Cem. Concr. Res. 33 (2003) 133–138.
[11] M.R. Geiker, Fly Ash in Concrete, Danish Experience: State-of-the-art Report, (2015).
[12] K. De Weerdt, D. Orsáková, A.C.A. Müller, C.K. Larsen, B. Pedersen, M.R. Geiker, Towards the understanding of chloride profiles in marine exposed concrete, impact of leaching and moisture content, Constr. Build. Mater. 120 (2016) 418–431.
[13] K. De Weerdt, H. Justnes, M.R. Geiker, Changes in the phase assemblage of concrete exposed to sea water, Cem. Concr. Compos. 47 (2014) 53–63.
[14] U.H. Jakobsen, K. de Weerdt, M.R. Geiker, Elemental zonation in marine concrete, Cem. Concr. Res. 85 (2016) 12–27.
[15] P. Hemstad, pH-dependence of Chloride Binding in Ordinary Portland Cement, Master thesis, Trondheim, Norway (2018).
[16] A. Machner, P. Hemstad, K. De Weerdt, Towards the understanding of the pH dependency of the chloride binding of Portland cement pastes, Nord. Concr. Res. 58 (2018) 143–162.
[17] K.L. Scrivener, H.F.W. Taylor, Delayed ettringite formation: a microstructural and microanalytical study, Adv. Cem. Res. 5 (1993) 139–146.
[18] H.F.W. Taylor, C. Famy, K.L. Scrivener, Delayed ettringite formation, Cem. Concr. Res. 31 (2001) 683–693.
[19] M.H. Roberts, Effect of calcium chloride on the durability of pre-tensioned wire in prestressed concrete, Mag. Concr. Res. 14 (1962) 143–154.
[20] A.K. Suryavanshi, R.N. Swamy, Stability of Friedel's salt in carbonated concrete structural elements, Cem. Concr. Res. 26 (1996) 729–741.
[21] M. Balonis, B. Lothenbach, G. Le Saout, F.P. Glasser, Impact of chloride on the mineralogy of hydrated Portland cement systems, Cem. Concr. Res. 40 (2010) 1009–1022.
[22] C. Labbez, A. Nonat, I. Pochard, B. Jönsson, Experimental and theoretical evidence of overcharging of calcium silicate hydrate, J. Colloid Interface Sci. 309 (2007) 303–307.
[23] G. Plusquellec, A. Nonat, Interactions between calcium silicate hydrate (C-S-H) and calcium chloride, bromide and nitrate, Cem. Concr. Res. 90 (2016) 89–96.
[24] J. Tritthart, Chloride binding in cement II. The influence of the hydroxide concentration in the pore solution of hardened cement paste on chloride binding, Cem. Concr. Res. 19 (1989) 683–691.
[25] C.M. Hansson, T. Frølund, J.B. Markussen, The effect of chloride cation type on the corrosion of steel in concrete by chloride salts, Cem. Concr. Res. 15 (1985) 65–73.
[26] H.F.W. Taylor, Cement Chemistry, (1990).
[27] Z. Shi, M.R. Geiker, K. De Weerdt, T.A. Østnor, B. Lothenbach, F. Winnefeld, J. Skibsted, Role of calcium on chloride binding in hydrated Portland cement–metakaolin–limestone blends, Cem. Concr. Res. 95 (2017) 205–216.
[28] Q. Zhu, L. Jiang, Y. Chen, J. Xu, L. Mo, Effect of chloride salt type on chloride binding behavior of concrete, Constr. Build. Mater. 37 (2012) 512–517.
[29] K. De Weerdt, A. Colombo, L. Coppola, H. Justnes, M.R. Geiker, Impact of the associated cation on chloride binding of Portland cement paste, Cem. Concr. Res. 68 (2015) 196–202.
[30] A. Machner, M. Zajac, M.B. Haha, K.O. Kjellsen, M.R. Geiker, K. De Weerdt, Chloride-binding capacity of hydrotalcite in cement pastes containing dolomite and metakaolin, Cem. Concr. Res. 107 (2018) 163–181.
[31] I. Pointeau, P. Reiller, N. Macé, C. Landesman, N. Coreau, Measurement and modeling of the surface potential evolution of hydrated cement pastes as a function of degradation, J. Colloid Interface Sci. 300 (2006) 33–44.
[32] M. Balonis, The Influence of Inorganic Chemical Accelerators and Corrosion Inhibitors on the Mineralogy of Hydrated Portland Cement Systems, PhD, Aberdeen, Scotland (2012).

[33] G. Plusquellec, M.R. Geiker, J. Lindgård, B. Fournier, K. De Weerdt, Determination of the pH and the free alkali content in the pore solution of concrete: review and experimental comparison, Cem. Concr. Res. 96 (2017) 13–26.
[34] B. Lothenbach, P. Durdzinski, K. De Weerdt, Thermogravimetric analysis, in: K.L. Scrivener, R. Snellings, B. Lothenbach (Eds.), A Practical Guide to Microstructural Analysis of Cementitious Materials, CRC Press, 2015.
[35] A. Machner, M. Zajac, M. Ben Haha, K.O. Kjellsen, M.R. Geiker, K. de Weerdt, Stability of the hydrate phase assemblage in Portland composite cements containing dolomite and metakaolin after leaching, carbonation, and chloride exposure, Cem. Concr. Compos. 89 (2018) 89–106.
[36] K. De Weerdt, D. Orsáková, M.R. Geiker, The impact of sulphate and magnesium on chloride binding in Portland cement paste, Cem. Concr. Res. 65 (2014) 30–40.
[37] D.A. Kulik, T. Wagner, S.V. Dmytrieva, G. Kosakowski, F.F. Hingerl, K.V. Chudnenko, U.R. Berner, GEM-Selektor geochemical modeling package: revised algorithm and GEMS3K numerical kernel for coupled simulation codes, Comput. Geosci. 17 (2013) 1–24.
[38] T. Wagner, D.A. Kulik, F.F. Hingerl, S.V. Dmytrieva, GEM-Selektor geochemical modeling package: TSolMod library and data interface for multicomponent phase models, Can. Mineral. 50 (2012) 1173–1195.
[39] D.A. Kulik, GEM-Selektor v.3.3, http://gems.web.psi.ch/.
[40] D.A. Kulik, Improving the structural consistency of C-S-H solid solution thermodynamic models, Cem. Concr. Res. 41 (2011) 477–495.
[41] S. Sui, W. Wilson, F. Georget, H. Maraghechi, H. Kazemi-Kamyab, W. Sun, K. Scrivener, Quantification methods for chloride binding in Portland cement and limestone systems, Cem. Concr. Res. 125 (2019) 105864.
[42] K.L. Scrivener, A. Bazzoni, B. Mota, J.E. Rossen, Electron microscopy, in: K.L. Scrivener, R. Snellings, B. Lothenbach (Eds.), A Practical Guide to Microstructural Analysis of Cementitious Materials, CRC Press, 2015.
[43] K.L. Scrivener, R. Snellings, B. Lothenbach (Eds.), A Practical Guide to Microstructural Analysis of Cementitious Materials, CRC Press, 2015.
[44] R. Skapa, Optimum Sulfate Content of Portland Cement, PhD Thesis University of Aberdeen, Aberdeen, Scotland, UK, 2009.